minerals

MDPI

Article

Comparison of the Calcareous Shells of Belemnitida and Sepiida: Is the Cuttlebone Prong an Analogue of the Belemnite Rostrum Solidum?

M. Isabel Benito [1] and Matías Reolid [2,*]

[1] Departamento de Geodinámica, Estratigrafía y Paleontología, Fac. Cc Geológicas, IGEO (CSIC-UCM), 28040 Madrid, Spain; mibenito@ucm.es

[2] Departamento de Geología, Universidad de Jaén, Campus Las Lagunillas sn, 23071 Jaén, Spain

* Correspondence: mreolid@ujaen.es

Received: 30 June 2020; Accepted: 9 August 2020; Published: 12 August 2020

Abstract: The microstructure of the rostrum solidum of Jurassic belemnites is compared with that of *Sepia* cuttlebones, in order to examine possible convergences in their style of growth. For this study, transmitted and polarized light, cathodoluminescence, epifluorescence, scanning electron and backscattered electron microscopy have been employed. Despite differences in the primary mineralogy of the studied belemnites and sepiids, calcite and aragonite, respectively, many similarities have been observed between the microstructure of the belemnite rostra and the prong of *Sepia* cuttlebone: (1) In both, crystals start growing from successive spherulites, from which crystals emerge radially towards the apex and the external walls, displaying internally micro-fibrous texture. (2) Both display concentric growth layering, comprising an alternation of organic-rich and organic-poor layers, which, in turn, is traverse by the radially-arranged micro-fibrous crystals. (3) The highest organic matter content and porosity have been observed along the apical area of the *Sepia* prong, similarly to that interpreted for belemnite rostra. The strong convergences observed suggest that the growth of belemnites occurred similarly to that of the prong of sepiids and that the *Sepia* prong is the analog of the belemnite rostrum. Additionally, non-classical crystallization processes are proposed to be involved in the formation *Sepia* endoskeleton.

Keywords: crystal growth; organic matter; coleoids; microstructure; non-classical mineralization

1. Introduction

In addition to their usefulness for biostratigraphical studies, belemnite rostra are commonly used for palaeoclimatic, palaeobiological and palaeobiogeographical studies based on their geochemical data or on their morphological features [1–36]. However, no agreement exists regarding whether belemnites were originally porous [1,2,37–42], or whether the original porosity was of minor importance [43,44], although this issue has important implications for reconstructing, for example, their buoyancy, size and ontogenetic strategies and palaeoenvironments. Some authors have proposed low porosity values for belemnite rostra [3,7,29]. However, Veizer [2] and Spaeth [38] proposed up to 10% and 20% of primary porosity, respectively, for the belemnite rostrum, Ullmann et al. [41] up to 40% of porosity at the apical line, Hoffmann et al. [42] proposed 50–90% of porosity in belemnite rostra, and Benito et al. [31] proposed porosity values ranging from 20 to 60% in the apical area of the rostrum. In this regard, Benito et al. [31] also suggested that the analysis of the prong of *Sepia* cuttlebone could be useful for understanding the original structure and porosity of belemnite rostrum.

The fossil Order Belemnitida is included in the Subclass Coleoidea, though most recent coleoids have reduced their internal skeleton substantially or even entirely [36,45,46]. For example, it has been

interpreted that the chitinous squid gladius with septa-like layers in cone situated at the posterior end of the proostracum represents a vestigial phragmocone of ancient coleoids that has lost the siphuncle and gas-filled chambers, and that the "rostrum situated apically from the cone is homologous to the rostrum of ancient phragmocone-bearing coleoids" [47].

Belemnites have been interpreted as marine nekto-benthic dwellers [48] or as nektonic [49]. Sepiids are nekto-benthic dwellers and have retained a calcareous internal shell (cuttlebone) still used as a buoyancy device. However, the original mineralogy of sepiid cuttlebone differs from that of belemnites. The cuttlebone of *Sepia* is composed of aragonite [50–52]. Nevertheless, some authors have reported small amounts of primary calcite in modern sepiid cuttlebones [53,54] and in fossil sepioids [55]. Additionally, up to 70% of primary calcite has been reported by Yancey and Garvie [56] in Eocene *Anomalosaepia* specimens. The rostrum solidum of belemnites, on the contrary, was originally composed of low Mg-calcite [1,7,44,47,57–59]. However, some authors, based on petrographic and/or X-ray structural data, have interpreted that some belemnite rostra, such as those of various Jurassic Belemnoteuthidae and Turonian *Goniocamax*, were partially or totally composed of primary aragonite [60–64].

Despite the differences between their primary mineralogy, previous works have compared belemnites with cuttlebone, looking for homologies [65–72]. The prong or spine has been also named as rostrum by Naef [65], Dauphin [70] and Bizikov [73]. Abel [66] and Krymgol'ts [67] interpreted that the spine was not homologous to the belemnite rostrum. Naydin [68] observed clear homologies between some parts of the cuttlebone and the belemnite. For this author, the phragmocone, the fork (or ventral process) and the innermost layer of the dorsal shield are related to the belemnite phragmocone. Naydin [68] also interpreted that the middle and outermost layers of the dorsal shield and the prong (or spine) correspond to the belemnite rostrum. Barskov [69] interpreted that the middle layer of the dorsal shield corresponds to the belemnite rostrum, whereas Dauphin [70] interpreted that the outer layer of the dorsal shield and the spine corresponded to the belemnite rostrum. Naef [65] suggested that the belemnite rostrum and the *Sepia* prong are analogous organs and Rexfort and Mutterlose [48] proposed that "the sepioid rostrum, which is homologous to the belemnite guard, is purely organic". Additionally, the prong (or spine) has been associated with the middle layer of the dorsal shield [69,74], the outer layer of the dorsal shield [70] or seen as constituting an additional layer [73,75]. On the contrary, Fuchs [71] has interpreted that the rostrum is absent in Sepiida and that there is not an equivalent structure to the belemnite rostrum. In other cases, the comparison between *Sepia* and belemnites has been focused for understanding the belemnite palaeoecology from the study of stable isotopes of O and C on *Sepia officinalis* [48,76,77]. Finally, other authors have compared belemnite rostra with squids. Arkhipin et al. [47] indicated that the rostrum of the gladius of some squids (onychoteuthids, omnastrephids and gonatids) is homologous to the rostrum of belemnites *Hibolithes* and *Pachyteuthis*.

In this study, we compare the microstructure of the rostrum solidum of Jurassic belemnites *Hibolithes, Belemnopsis* and *Passaloteuthis* with that of cuttlefishes (*Sepia officinalis* and *S. orbignyana*) in order to examine if their style of growth is similar and check if the growth of the *Sepia* prong is similar to those of belemnite rostrum and can be considered as an analogous of the belemnite rostrum solidum.

2. Methods

This study is based on the analysis of 18 specimens of well-preserved Jurassic belemnite rostra (12 *Hibolithes*, 3 *Belemnopsis* and 3 *Passaloteuthis*; Figure 1) with that of 15 specimens of cuttlefishes (nine *Sepia officinalis* and six *S. orbignyana*; Figure 2) (see supplementary material for details, Table S1). The belemnites analyzed come from two outcrops located in the Betic Cordillera (South Spain). *Passaloteuthis* was recorded at La Cerradura section (lower Toarcian, Lower Jurassic, External Subbetic; see location on Figure 1 of Reolid et al. [78]) and *Hibolithes* and *Belemnopsis* were recorded at Pozo Cañada Section (Oxfordian-lowermost Kimmeridgian, Upper Jurassic, External Prebetic; see location on Figure 1 of Benito et al. [31]). Specimens of cuttlefishes come from the Alboran Sea (Western Mediterranean)

and the Cantabrian Sea, in the case of *S. officinalis*, and from the Alboran Sea, in the case of *S. orbignyana*. Polished and uncovered thin sections (30 and 400–500 μm thickness) were prepared for each belemnite rostrum (one longitudinal and one transversal to the growth of the belemnite rostra) and, when possible, one for each cuttlefish rostrum and prong which, in turn, were embedded in epoxy resin to make possible thin section preparations. The longitudinal sections were lateral and not oriented dorso-ventrally, except in one thin section. Ultra-thin sections (<15 mm thick) were also obtained after re-polishing three thin sections. Thin sections were studied and photographed under transmitted light (TL), polarized light (PL), cathodoluminescence (CL), and epifluorescence (FL) microscopy at the Universidad Complutense (Madrid): For CL study, a Technosyn cold cathodoluminescent unit MK4 at 20–24 kV with 350–400 mA beam current was employed; the FL study was carried out using an incident-light FL Nikon Y-FL epifluorescence system coupled to an Eclipse 6400 POL petrographic microscope. An UV (340–380 nm) excitation filter (400 nm dichroic mirror and 420 nm barrier filter) and a blue light (450–590 nm) excitation filter (505 nm dichroic mirror and 520 nm barrier filter). Specimens and thin sections are deposited in the collections of the Department of Geology of the University of Jaén.

Figure 1. Specimens of belemnites (*Hibolithes*) from the upper Oxfordian (Upper Jurassic) from Prebetic (Betic Cordillera, S. Spain). Specimens PC-39-25, PC-45-14 and PC-53-53. Scale bar 1 cm.

In terms of petrography, all the studied belemnite rostra are well-preserved and display transparent appearance under TL and lack of luminescence [30,31], despite the apical area and some growth layers of belemnites being diagenetically altered and displaying cloudy appearance and bright to dull luminescence (see Figures 2–5 in Benito and Reolid, [30] and Figure 6 in Benito et al. [31]). In this sense, Stevens et al. [33] have observed alternation of blue and orange luminescent growth lines in translucent brood cases of *Argonauta* and in belemnite rostra, which they interpret as primary. However, these authors also observed luminescent areas displaying cloudy appearance (under TL microscopy) in belemnite rostra, which they interpret as diagenetic in origin, in accordance with interpretations made by other authors [30,31,44,57].

Secondary electrons and backscattered scanning electron microscopy (SEM and BSEM, respectively) was performed using a JEOL JSM-820 electron microscope at the Universidad Complutense (Madrid, Spain) and a SCI Quanta 400 scanning electron microscope at the Centro de Instrumentación Científico-Técnica of the Universidad de Jaén (Spain), in both thin sections and in fresh-cut belemnites and cuttlefishes. Subsequently to examination, samples were etched after immersion in a 25% solution (Merck) of glutardialdehyde maintained at a pH of 4.0 for 12 h, in the case of thin sections, and 24 h in the case of fresh cut samples. Glutardialdehyde, $CH_2(CH_2CHO)_2$, is known to react with proteins [79]; moreover, because glutardialdehyde is easily oxidized to glutaric acid [80], it has been also benefited from the etching effect of the acid [35]. After treatment with glutardialdehyde, the slabs were washed with water and ethanol and then dried and analyzed under SEM.

Figure 2. Cuttlebones of specimen of *Sepia officinalis* (SP-07) and *S. orbignyana* (SP-11) studied in this work, observed in ventral (**up**) and dorsal view (**down**). Scale bar 1 cm. *Sepia* specimens were obtained in fisheries and their origin was the southern Spanish coast.

3. Results

3.1. Belemnitida

Belemnite shells are composed of three main parts: phragmocone, primordial rostrum and rostrum proper [71]. Longitudinally, they are also divided into proostracum, rostrum cavum and rostrum solidum (Figure 3). For checking the wide terminology for shell elements of belemnites [36,71]. Specimens of *Hibolithes* (Family Belemnopseidae) are characterized by an elongated and hastate rostrum, with the maximum transverse diameter at the posterior region, near the apex, a circular transverse section, and a shallow ventral groove limited at the anterior half of the rostrum. *Belemnopsis* (Family Belemnopseidae) presents a hastate and depressed rostrum, with maximum transverse diameter slightly posterior of the midpoint, an asymmetrical transverse section with ventral side inflated, and a deep broad ventral groove. The Toarcian specimens of *Passaloteuthis* (Family Passaloteuthididae) are characterized by a robust rostrum (with well-developed primordial rostrum), with cylindrical outline and a rounded to slightly compressed transverse section, without ventral grooves.

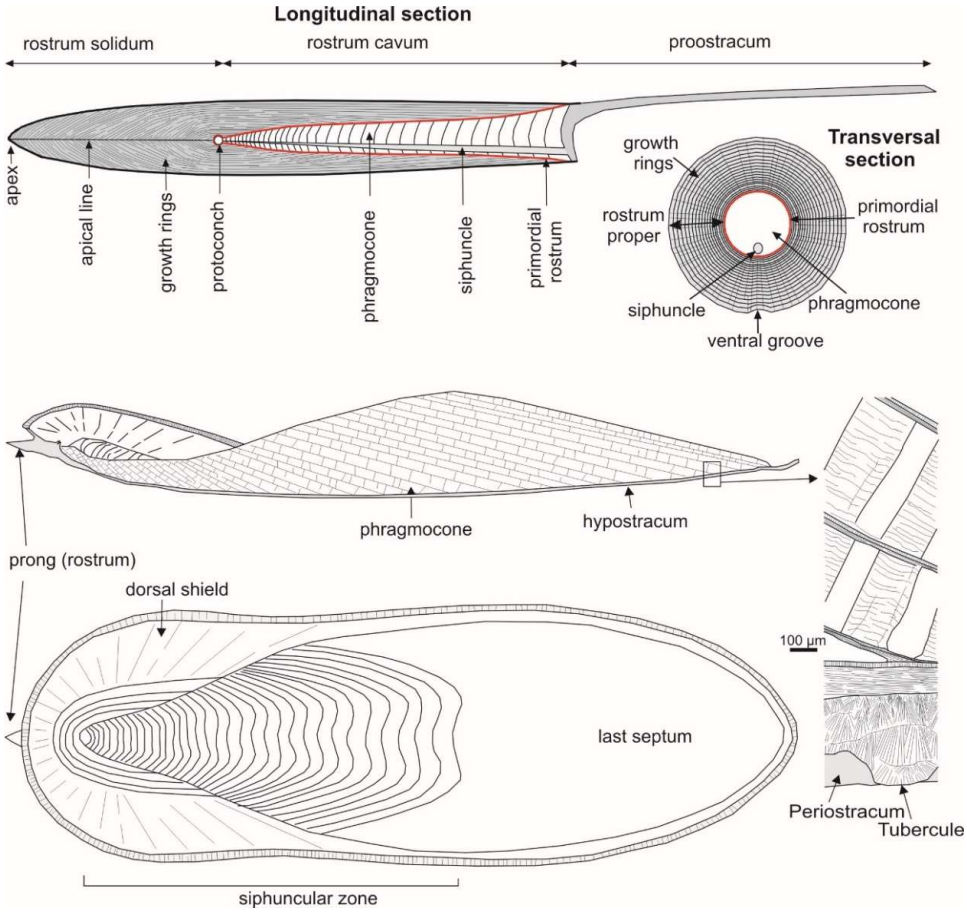

Figure 3. Sketch of the anatomy of the belemnite (**up**) and *Sepia* (**down**) endoskeleton. Red line indicates primordial rostrum.

The orthoconic phragmocone of *Hibolithes* and *Belemnopsis* opens at an angle of ca. 20° with the initial chamber of the protoconch (<0.6 mm diameter) completely sealed by a closing membrane and delimited by a slight constriction (Figures 3 and 4A). The phragmocone of *Passaloteuthis* opens at an angle of ca. 28°. The siphuncle penetrates the septa proper along their ventral margins (Figure 4). The phragmocone is enveloped by two calcitic external layers, the primordial rostrum (uni-layered and thin) and the rostrum proper (multi-layered and thick), as described by Fuchs [71] and Doguzhaeva et al. [81]. The primordial rostrum of these belemnite genera was originally aragonitic and contained abundant non-biomineralized components (probably chitin [81]). The rostrum solidum was originally composed of low Mg-calcite [2,7,44,47,57–59].

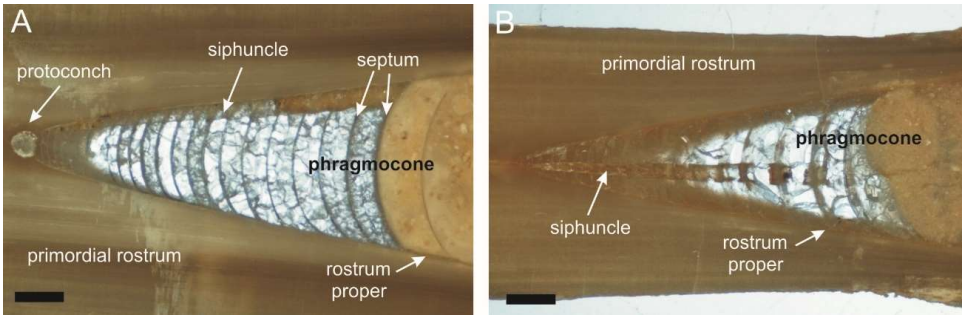

Figure 4. Examples of Oxfordian belemnites ((**A**) specimen PC-11-183; (**B**) specimen PC-11-31) showing the protoconch and the first chambers of the phragmocone, which are infilled by sparitic calcite cement. Scale bar 1 mm.

The belemnite rostrum solidum, when observed under the petrographic microscope in both transversal and longitudinal sections, is formed by radially arranged prismatic calcite crystals, which emerge from the apical line, and display a concentric pattern (Figure 5), commonly interpreted as growth layers or rings [30,31,44,82,83], and undulose extinction under polarized light (PL) microscopy (Figure 5B,E). The rostrum solidum is also characterized by a regular spherulithic prismatic microstructure [31] formed by spherulites of around 250 μm in diameter that successively develop along the apical line and from which calcite crystals radially emerge and diverge, as is observed in the longitudinal sections of the rostra under SEM, as well as under PL microscopy in the ultra-thin sections (Figure 6). The inner parts of the spherulitic centers are composed by dense concentrations of small calcite crystals (<1 μm in the nuclei of the spherulithic centers). Progressively, calcite crystals become larger and more elongated and radially distributed as hemispheric fans (Figure 6B,C). Towards the outer parts of the rostra, crystals become longer, thicker and prismatic in shape (Figure 6).

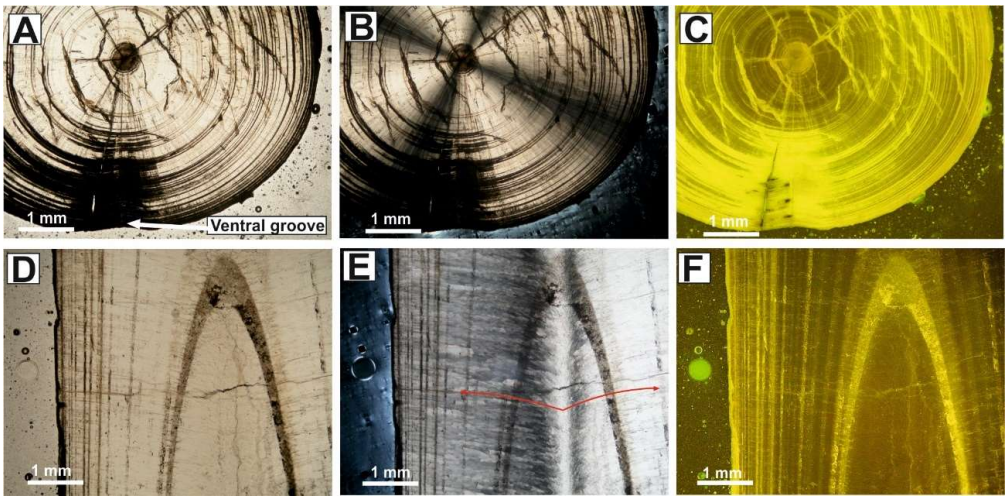

Figure 5. Transversal (**A**–**C**) and longitudinal (**D**–**F**) thin sections of the same belemnite rostrum (specimen PC-39) observed under TL (**A**,**D**), PL (**B**,**E**), and FL (**C**,**F**) microscopy. Note the concentric growth layering, enhanced under FL, and the undulose extinction, under PL. Red arrows observed in (**E**) indicate the sense of crystal growing from the apical line.

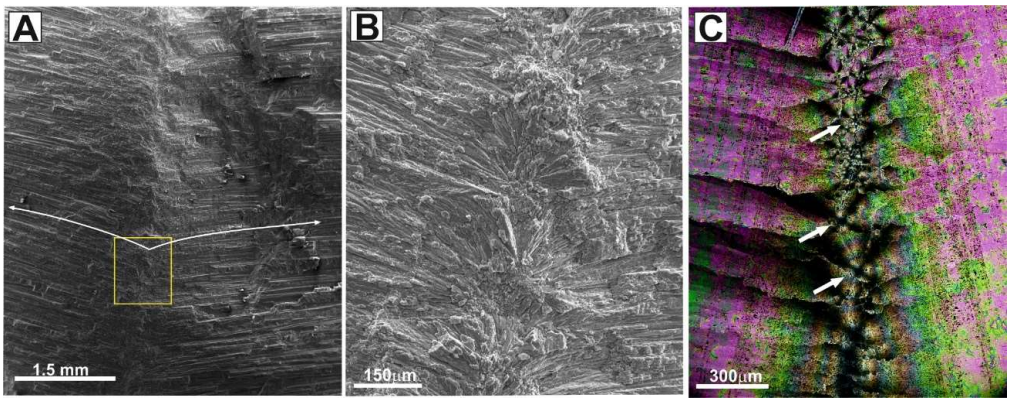

Figure 6. Photographs showing spherulites developed along the apical line in belemnite rostra. (**A**) SEM images of longitudinal fresh cut sample showing the apical line and the area where spherulites are observed (specimen PC-39). White arrows indicate the sense of crystal growing from the apical line. (**B**) Detail of A showing the spherulites. They are composed of radially arranged calcite crystals. Crystals become progressively longer and prismatic towards the external walls of the rostrum (**A**). (**C**) Ultra-thin section observed under PL microscopy (PC-31-04). Spherulites are observed along the apical line (white arrows). Note that prismatic crystals traverse the concentric growth layering and display micro-fibrous texture and undulose extinction.

The detailed examinations of the calcite prisms also allow to differentiate an internal micro-fibrous texture, which is observable under TL, PL, FL, SEM and BSEM (Figure 7), and is enhanced after etching with 25% glutardialdehyde (Figure 8) [31,44]. The concentric pattern, which may be also observed at different scales, is traversed by the radial pattern (Figures 5, 7 and 8B) and is enhanced under FL microscopy and BSEM (Figure 7C,G,H). Some concentric layers (10–50-μm thick, generally) display an internal radial micro-fibrous texture, weak FL and an overall light grey colour under BSEM. These layers are separated by very thin concentric layers (<5 μm thick), which display intense FL and an overall dark grey colour under BSEM. Benito et al. [31] also observed that single calcite crystals of belemnite rostra are composite and are composed of two sectors, which are in optical continuity (Figure 9A–J): an inner sector, fluorescent, with relatively low optical relief under TL microscopy, and a dark-grey colour under BSEM, which may have an internal "patchy" appearance (Figure 9G–I), and an outer sector, non-fluorescent, with relatively high optical relief under TL, and a light-grey colour under BSEM. These sectors may be also observed after etching thin sections with 25% glutardialdehyde (Figure 9K–L). The composite nature of belemnite crystals has been also suggested or interpreted by other authors, such as Richter et al. [84] and Hoffman et al. [36], respectively, for other Jurassic and Cretaceous belemnite species (*Belemnitella*, *Cylindroteuthis*, *Gonioteuthis*, *Megateuthis*, and *Pachyteuthis*). Additionally, Benito and Reolid [30] and Benito et al. [31] observed that the concentric layers and sectors of the crystals displaying intense FL also had higher Mg, Na and S concentrations than those showing weak or no FL.

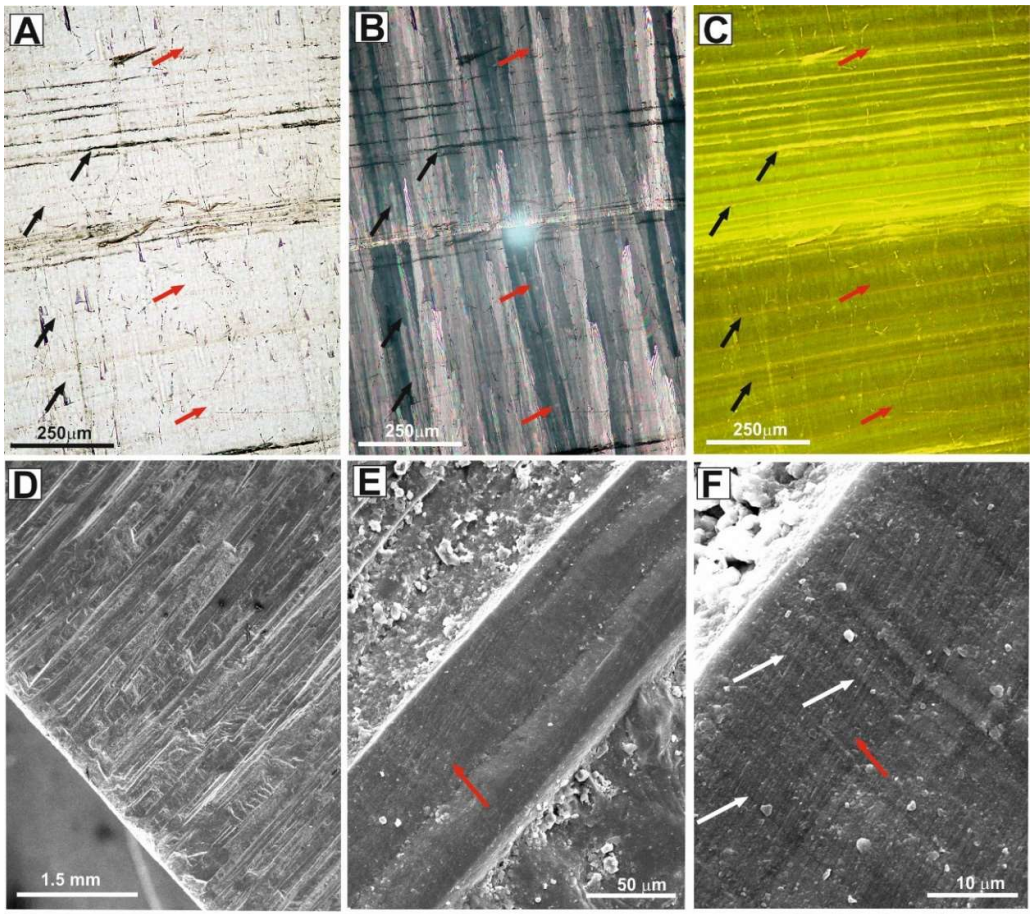

Figure 7. *Cont.*

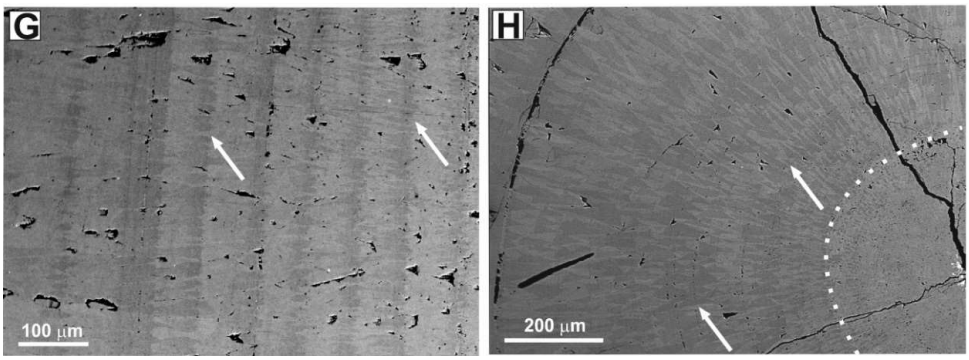

Figure 7. Details of the micro-fibrous texture of the prismatic crystals and the concentric layering of belemnite rostra. (**A**–**C**) Longitudinal thin section under TL (**A**), PL (**B**) and FL (**C**) microscopy (specimen PC-31-04) showing the micro-fibrous texture of the crystals (black arrows) and the concentric layering. Under FL, the concentric layering is enhanced: some layers display weak FL and micro-fibrous texture; they are separated by very thin and intense FL layers, in which the micro-fibrous texture is no evident. (**D**–**F**) Transversal fresh-cut sample (CE-25-04) under SEM. Prismatic crystals of calcite internally display a micro-fibrous texture ((**E**,**F**) red arrows). Perpendicular growth layering is also observable. Note that microfibers traverse the concentric growth layering ((**F**) white arrows). (**G**,**H**) Longitudinal (**G**) and transversal (**H**) thin sections (specimens PC-31-04 and PC-37-01, respectively) observed under backscattered (**B**) SEM. The micro-fibrous texture is observable as fibers displaying alternating light- and dark- grey colours. Note that the light-grey fibers traverse the concentric growth layers displaying an overall dark-grey colour (white arrows), which correspond to the thin layers that displays intense FL (see (**C**)). Note also that, in transversal sections (**H**), the micro-fibrous texture is not observable in the inner part of the rostra (in the apical area) but progressively becomes more evident towards the external wall of the rostra.

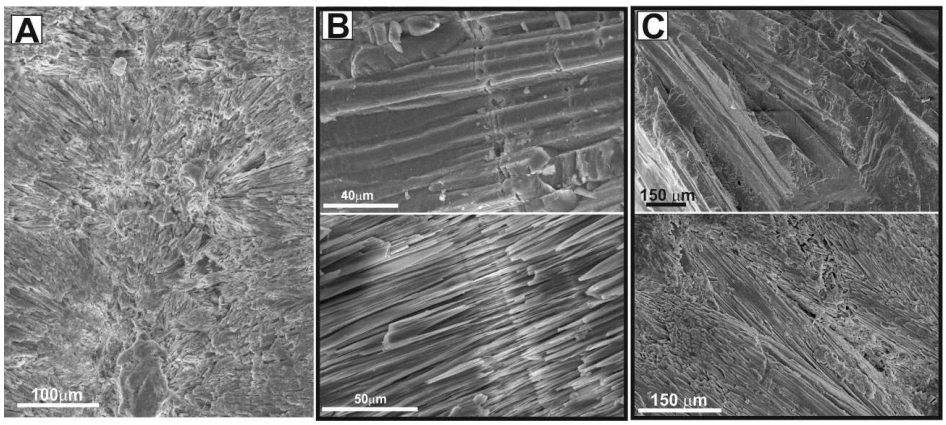

Figure 8. SEM images of fresh-cut samples of belemnite rostra after etching with 25% glutardialdehyde. Note that the micro-fibrous texture is enhanced after etching. (**A**) Equivalent image to 6B showing the spherulites developed along the apical line after etching. (**B**,**C**) Transversal (**B**) and longitudinal (**C**) sections of specimens PC-39 and CE-25-04, respectively, showing the prismatic habit of crystals (**up**), and the equivalent image after etching (**down**). Note that fibers traverse the concentric layers (**B**).

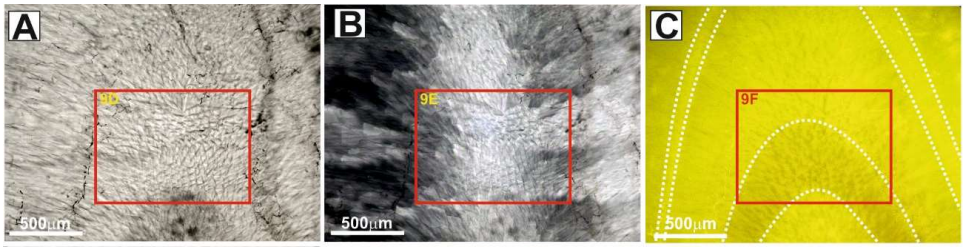

Figure 9. *Cont.*

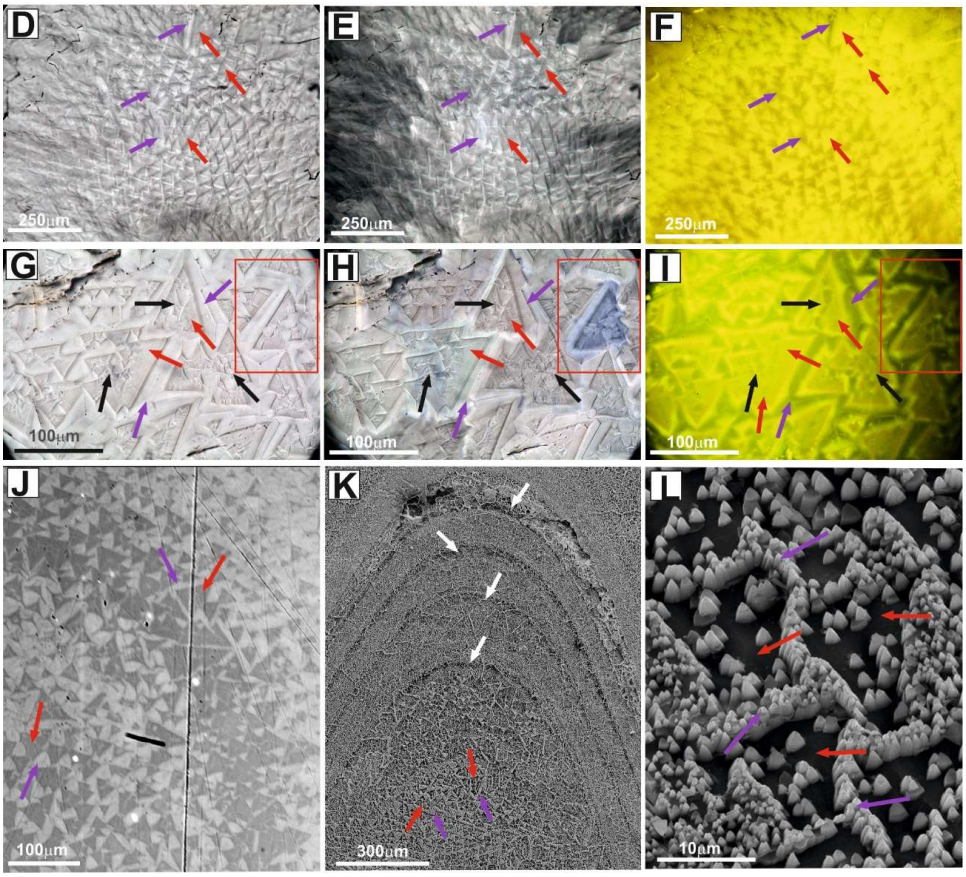

Figure 9. Photographs showing the composite nature of calcite crystals in belemnite rostra, which is observed in longitudinal sections that do not cross-cut the rostrum along the apical line. (**A**–**C**) TL (**A**), PL (**B**) and FL (**C**) photographs (specimen PC 31-4). In the central area, calcite crystals are cut perpendicularly to their c-axis and they are observed as an equigranular mosaic of crystals. Outwards, towards the external wall, crystals are cut tangentially to their c-axis and become elongated. Note also that the concentric layering is enhanced under FL microscopy and that layers become thinner towards the external walls. (**D**–**F**) Detailed images of (**A**–**C**). Note the triangular shape of crystals that comprise sectors displaying relatively low optical relief (**D**,**E**) and intense FL (**F**) (red arrows) and sectors displaying relatively high optical relief (**D**,**E**) and none-to-weak FL (**F**) (purple arrows). (**G**–**I**) Detailed photographs showing the composite nature of calcite crystals under TL (**G**), PL (**H**) and FL (**I**) microscopy (specimen PC-11-31). Triangular-shaped crystals comprise an inner sector (red arrows), which displays an overall relatively low optical relief (**D**,**E**), intense FL (**F**) and an internal "patchy" appearance (black arrows). Note that the "patches" also displays a triangular shape and higher optical relief than the surrounding calcite. The outer sector of the crystals (purple arrows), which is in optical continuity with the inner sector (red square in (**H**)), displays relatively high optical relief (**D**,**E**) and non-to weak FL (**F**). Note the crystal boundaries (purple arrows and red square in (**G**) and (**H**)). Note also that the triangular "patches" of the inner sector has an identical optical relief and FL than the outer sector of the crystals. (**J**) Same thin section as in (**A**–**F**), observed under BSEM. The triangular inner sectors of the crystal displaying intense FL are dark-grey in colour (red arrows), and the outer sectors of the crystals, displaying non-to weak FL, are light-grey in colour (purple arrows). (**K**,**L**). Same thin section as in (**A**–**G**), observed under BSEM after etching with 25% glutardialdehyde. Note that the triangular shape of crystals and the concentric layering (white arrows in (**K**)) is enhanced under etching. The triangular areas comprise an inner sector, which has been largely etched (red arrows), and an outer sector where dissolution is less pervasive (purple arrows). The largely etched concentric layers, which would correspond to the intense FL concentric layers, are thin (white arrows) compared to those where etching is less pervasive.

3.2. Sepiida

The cuttlebone of *Sepia* is composed of aragonite, coated with a thin layer of organic matter, and encased by an epithelium also called the cuttlebone sac [48,85]. The cuttlebone is composed of three different parts, the phragmocone, the dorsal shield and the prong (Figures 3 and 10).

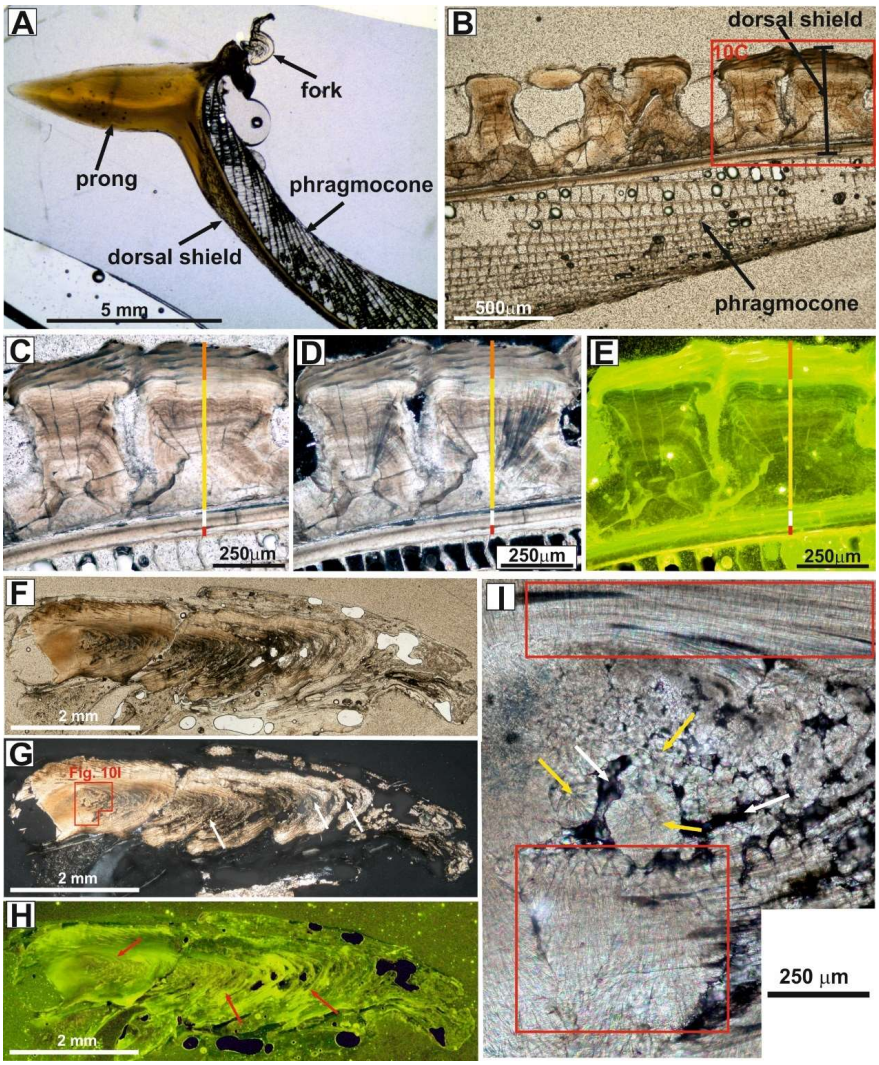

Figure 10. Thin sections of *Sepia*. (**A**) *S. orbignyana*. (**B**–**I**) *S. officinalis*. (**A**) Cuttlebone of S. *orbignyana* (SP-12) under magnification glasses showing the phragmocone, the dorsal shield and the prong. (**B**) Phragmocone and dorsal shield under TL microscopy (SP-07) with the tubercles. (**C**–**E**) Detailed view of (**B**), under TL (**C**), PL (**D**), and FL (**E**). The dorsal shield comprises 3 layers: the inner (red bar), displaying weak FL, the middle layer (white bar), displaying intense FL, and the outer layer (yellow and orange bars). The outer layer, which forms the tubercles and displays undulose extinction and concentric layering, comprises an inner part (yellow bar) composed of radially arranged aragonite crystals displaying non- to weak FL (despite its internal FL concentric pattern), and an outer part (orange bar) displaying very intense FL. (**F**–**I**) Longitudinal thin section of the prong under TL (**A**), PL (**B**,**I**) and FL (**C**) microscopy (SP-01). The red square on G represents the area shown in (**I**). Note the concentric growth pattern of the prong (red arrows in (**H**)), and the high intra-skeletal porosity (white arrows in (**G**) and (**I**)), which is enhanced in the apical area. Spherulites are developed in the inner part of the prong (yellow arrows), displaying radially arranged aragonite crystals and undulose extinction. Towards the outer wall of the prong, aragonite crystals become longer and radially arranged, displaying undulose extinction and traversing the concentric layering (red squares). Modified from Figure 7 of Benito et al. [31], who erroneously assigned this specimen to *S. orbignyana.*

The phragmocone contains many spaced septae (around 400 in *Sepia officinalis* [48]), connected by small undulating transverse pillars (undular plates [69], or palisades [44]) (Figures 10A,B and 11). The septae are connected to the inner mineralized layer of the dorsal shield and extend rearward from it (Figure 11B,C). The septae are composed of two layers: the anterior (~9 μm) is of prismatic structure with fine and densely arranged parallel prisms, which are perpendicular to the septum; the posterior layer is lamellar (~15 μm; Figure 11F).

The analysis of septae under BSEM allowed to recognise that the lamellar layer is richer in organic matter than the prismatic layer. In detail, the lamellar layer is composed of an alternation of organic- and aragonitic-rich sublayers (Figure 11G). The transverse pillars are made up of laminae composed of small randomly oriented aragonite crystals [69] that, under BSEM, show an internal alternation of organic-rich and organic-poor laminae (Figure 11E). In *S. officinalis,* the heights of the transverse pillars range between 490 and 150 μm, meanwhile in *S. orbignyana* they range between 195 and 80 μm. According to Florek et al. [86], septa are richer in β-chitin and pillars in aragonite. Organic films are also observed between septae (Figure 11D,H,I).

The chambered cuttlebone has a dual function as a support and as buoyancy regulation through liquid and gas adjustments, which requires an open structure that is pressure-resistant while maintaining a constant volume [87]. The porosity of the cuttlebone of *S. officinalis* is 93% [88], although *Sepia* species that live in deeper habitats had thicker septa and less space between pillars than shallow species [89].

The dorsal shield (Figures 10A–E and 12) contains high organic matter content and has an important mechanical role by increasing the flexural strength of the cuttlebone at the same time that has high porosity and high permeability [87,88]. In the case of *S. officinalis*, the phragmocone contains 10% of organic matrix and the dorsal shield 30–40% [86,88]. Dorsal shield occupies the dorsal region of the cuttlebone, above the phragmocone, and comprises three mineralized layers [69,70] (Figures 3, 10C–E and 12). The outer layer consists of convex outwards hemispheres composed of radially arranged acicular crystals of aragonite, which display undulose extinction under PL microscopy and concentric layering of alternating non- to intense FL (Figures 10C–E and 12B–G). The hemispheres constitute the tubercles in the surface of the dorsal shield of *S. officinalis* but, in *S. orbignyana,* tubercles are poorly developed. The thickness of the outer layer is variable along the dorsal shield, ranging between 315 and 411 μm and the contact with the middle layer is stepped in the proximal parts of the cuttlebone in *S. officinalis*. Over the outer mineralized layer of the dorsal shield, there is an organic granulated layer (170 μm maximum thick), which is highly porous and displays intense FL (Figures 10C–E, 11B,C and 12D).

The middle layer of the dorsal shield (Figure 10C–E) presents a laminated structure (Figure 12H–J) composed of organic-rich lamellar sublayers (1.5 μm) alternating with prismatic sublayers of aragonite (4–5 μm). The distribution of organic matter is clearly observed under BSEM (Figure 12C). The thickness of the middle layer is variable along the dorsal shield and displays a stepped distribution with a thinner middle layer of about 50–60 μm, and it becomes progressively thicker, reaching 95–130 μm. In addition, the middle layer is thinner in the distal parts of the cuttlebone.

The prong or spine (also called mucron by Cuif et al. [90]) is a solid tooth-like continuation of the middle layer of the dorsal shield, according to Barskov [69] (Figures 3, 10A,F–H and 13). Dauphin [91] proposed that the *Sepia* spine consists of the same three layers which form the dorsal shield, with the inner and middle ones being very thin. In our samples, we have not observed these layers in the spine from *S. orbignyana* and *S. officinalis*. The prong is comparatively better developed in *S. orbignyana* (7.6–11.2% of the total length) than in *S. officinalis* (1.5–2.7% of the total length) (Figure 2). In transversal sections, the prong is composed of alternating concentric laminae of aragonite crystals, displaying radial arrangement, and organic-rich and very thin laminae (Figure 13B). In a close view, the aragonite crystals are composed of clusters of small crystalline units (Figure 13B) with rod-like appearance. To the outer parts of the prong, aragonite crystals are progressively more elongated and become parallel (Figure 14), displaying a similar microstructure to that observed in transversal sections of the belemnite rostra (compare Figures 7E,F,H, 13B and 14).

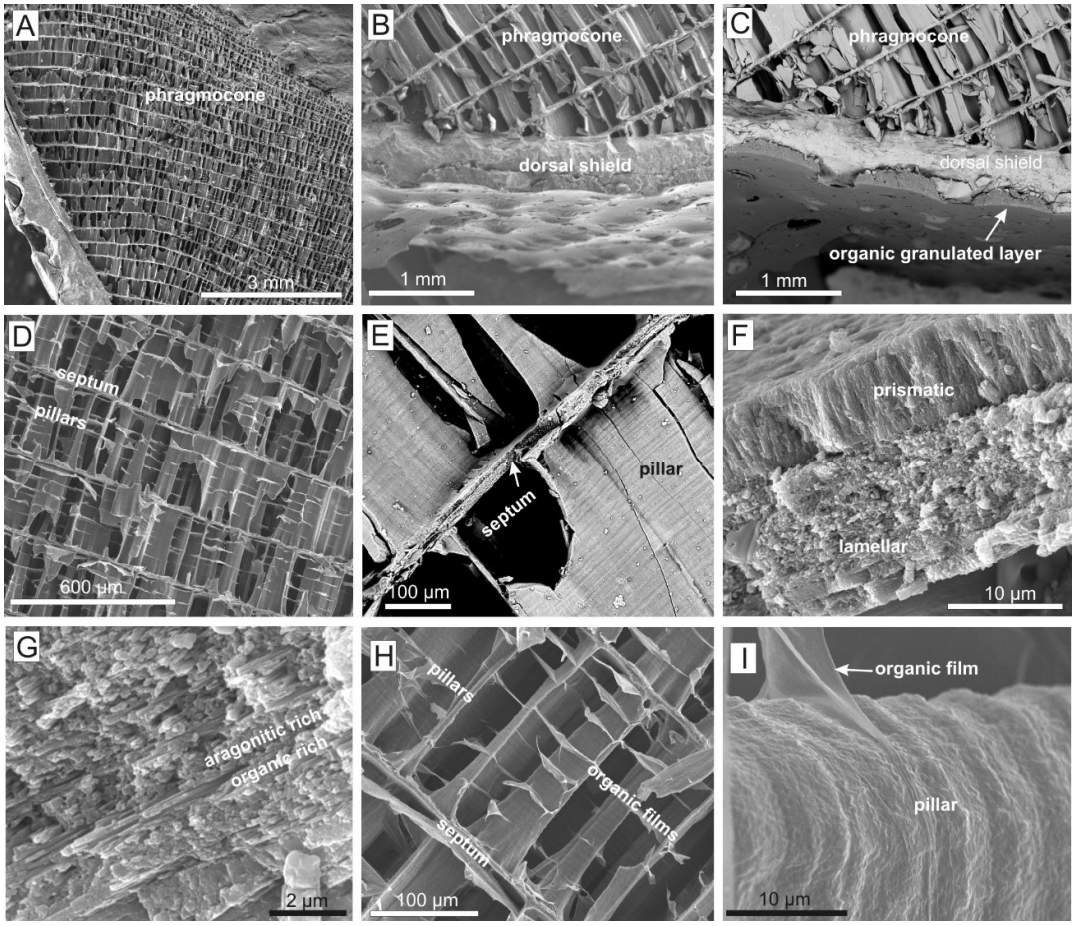

Figure 11. Phragmocone structure of *Sepia.* (**A**) Distal end of cuttlebone with contact between dorsal shield and youngest chambers of the phragmocone (SP-10). (**B**) General view of the phragmocone and the dorsal shield of *Sepia officinalis* under the SEM (SP-07). (**C**) General view of the phragmocone and the dorsal shield of *S. officinalis* under BSEM (SP-02); note that the organic granulated layer is darker than the rest of the dorsal shield. (**D**) Detail of the phragmocone of *S. officinalis* (SP-03) composed by septae supported by undulating transverse pillars or palisades. (**E**) BSEM image (SP-02) of undular plates with alternating dark (organic rich) and white (aragonite rich) layers. (**F**) Detailed view of a septum (SP-07) composed of two layers, the anterior (~9 µm) is of prismatic structure with fine and densely arranged prisms perpendicular to the septum, and the posterior layer is lamellar (~15 µm). (**G**) Lamellar layer is composed of an alternation of organic and aragonitic-rich sublayers (SP-07). (**H**,**I**) Detail of the pillars between septae showing the rhythmic growth as well as the presence of organic films (SP-07).

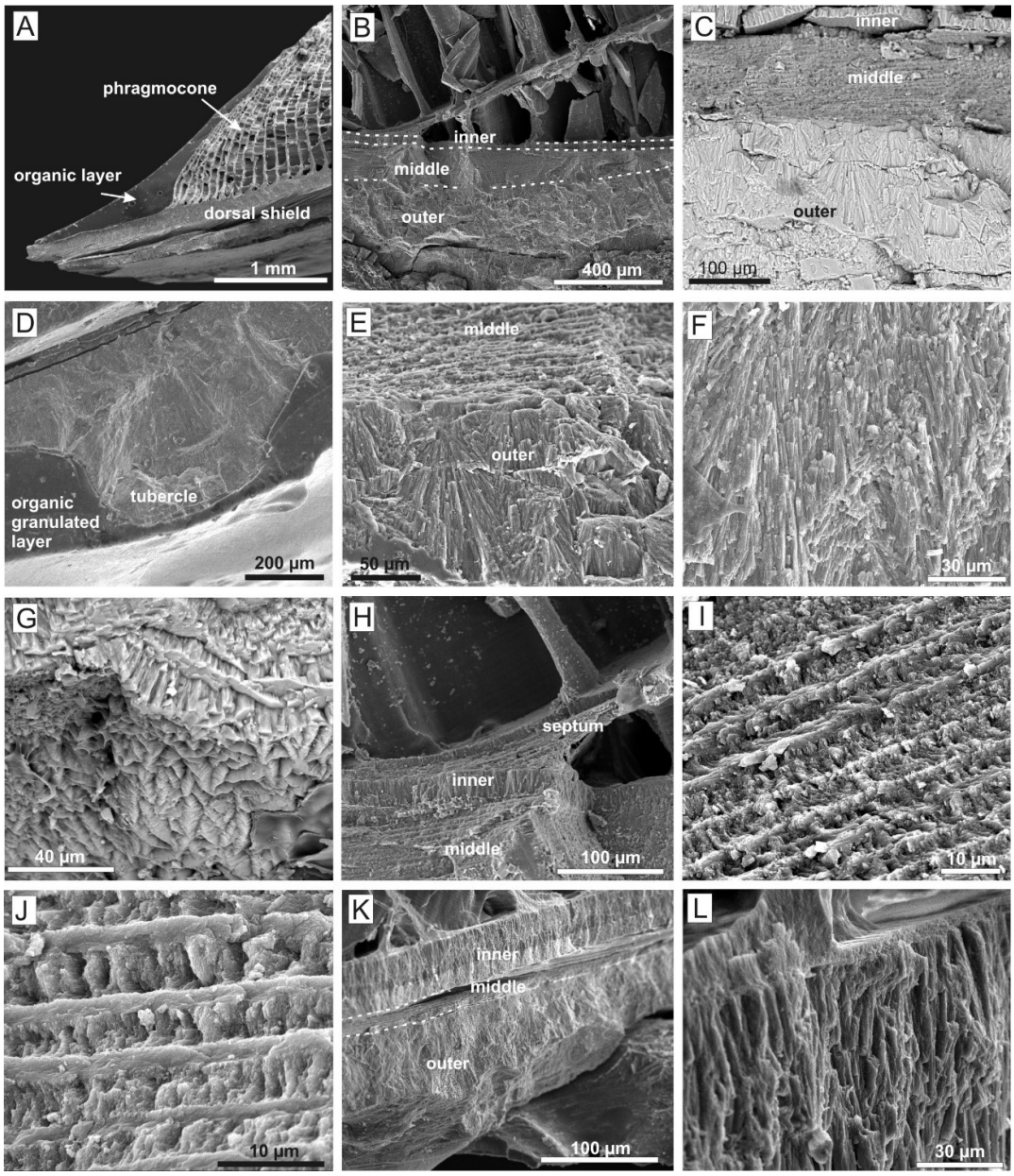

Figure 12. SEM images of the dorsal shield of *S. officinalis*. (**A**) Distal end of the cuttlebone (SP-03) with the contact between dorsal shield and the youngest chambers of the phragmocone. (**B**) The three mineralized layers of the dorsal shield, from the inner one, close to the phragmocone, to the outer one, in contact with the organic layer (SP-03). (**C**) BSEM image (SP-02) of the mineralized layers: the inner layer (prismatic microstructure); the middle layer (laminated microstructure, composed of organic-rich lamellar sublayers alternating with aragonitic prismatic sublayers); the outer layer (radially arranged crystals of aragonite with low presence of organic matter). (**D**) Outer layer with presence of tubercles in the contact with the external organic granulated layer (SP-07). (**E**) Differences between the microstructure of the outer and the middle layers (SP-07). (**F**,**G**) Radially arranged aragonite crystals of the outer layer (SP-07), which resemble hemispheres (**G**). (**H**) Prismatic microstructure of the inner layer and structural relation with the septum and the middle layer of the dorsal shield (SP-07). (**I**,**J**) Laminated structure of the middle layer with alternating organic-rich and aragonitic-rich sublayers (SP-07). (**K**,**L**) BSEM image in the distal part of the cuttlebone where the middle layer is very thin (SP-07). Radially arranged crystals of the inner layer growth from the middle layer to the phragmocone (laminated appearance due the organic matter content).

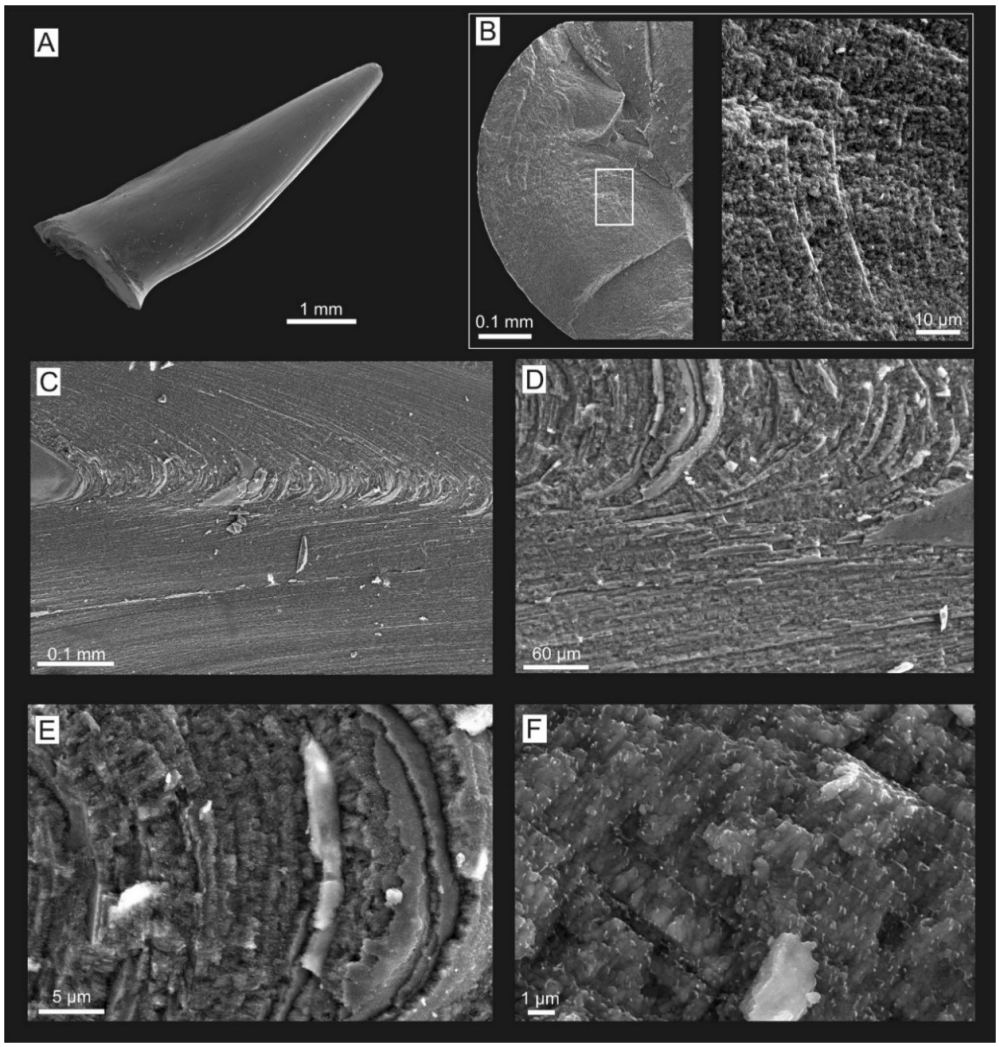

Figure 13. SEM images of the prong or spine of *Sepia orbignyana*. (**A**) General view of the prong (specimen SP-11). (**B**) Transversal section of the prong displaying fibrous and radial aragonite crystals distributed in concentric laminae (SP-12). (**C**–**E**) Longitudinal section (SP-14) showing the concentric laminae, which is parallel to the prong surface, and has the maximum curvature along the apical area (**C**–**E**). (**E**) Detailed image of (**D**), showing the concentric layering with and alternation of relatively thick aragonite-rich layers, and relatively very thin organic-layers. (**F**) Detail of the aragonite crystals displaying rod-like appearance and containing short organic fibers among them.

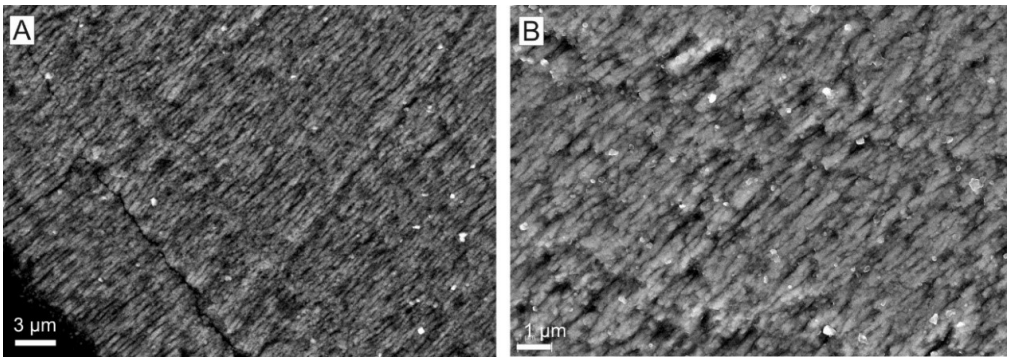

Figure 14. (**A**,**B**) SEM images of a transversal thin section of a prong of *S. officinalis* (SP-10) showing micro-fibrous texture of the crystals, which are distributed in concentric laminae.

In longitudinal sections, the prong is also composed of concentric laminae, which are parallel and younger towards the prong surface, similarly to that observed in longitudinal sections of belemnite rostra (compare Figures 5D–F, 9H, 10F–I and 13C–E). The highest porosity has been observed along the area where laminae have their maximum curvature (c.f. the apical area). In detail, under FL microscopy, concentric laminae of the *Sepia* prong are composed of alternating intense and non-to weak FL laminae (Figure 10H); under SEM relatively thick and organic-poor (aragonite-rich) laminae (2–5-µm-thick in the apical area) alternate with relatively thin and organic-rich laminae (0.5–1-µm-thick) (Figures 13D,E and 15). The overall thickness of the laminae decreases from the curved apical area to the straight lateral margins, similarly to that observed in belemnite rostra (compare Figures 5D–F, 9H, 10F,I and 13C–E). Some laminae in the apical area pinch out laterally and disappear (Figure 15A). Moreover, in longitudinal sections of the prong of *S. officinalis*, spherulites of radially arranged acicular crystals of aragonite have been observed in the inner area of the prong (Figure 10F,I). However, it has not been possible to observe the arrangement of spherulites properly, because of the difficulty in obtaining a section completely parallel to the apical area of the prongs. Aragonite crystals, which display undulose extinction under PL microscopy, become progressively longer towards the external wall of the prong, crossing-cut through different concentric laminae, similarly to that occurring in belemnite rostra (compare Figures 5E, 6C, 7A–C,G and 10I). However, under SEM it can be observed that radially arranged crystals are internally composed of clusters of nannometer-sized aragonite crystalline units (Figure 13E,F). In *S. orbignyana*, organic fibers (500 nm length, 60 nm diameter) are observed among the aragonite crystalline units, which may be aligned, displaying a poorly developed concentric layering (Figure 13F). In the case of *S. officinalis*, concentric thin organic films (<50 nm), comprising organic fibers, which are projected out, are observed interlayered with the aragonite crystalline units (Figure 15B–D).

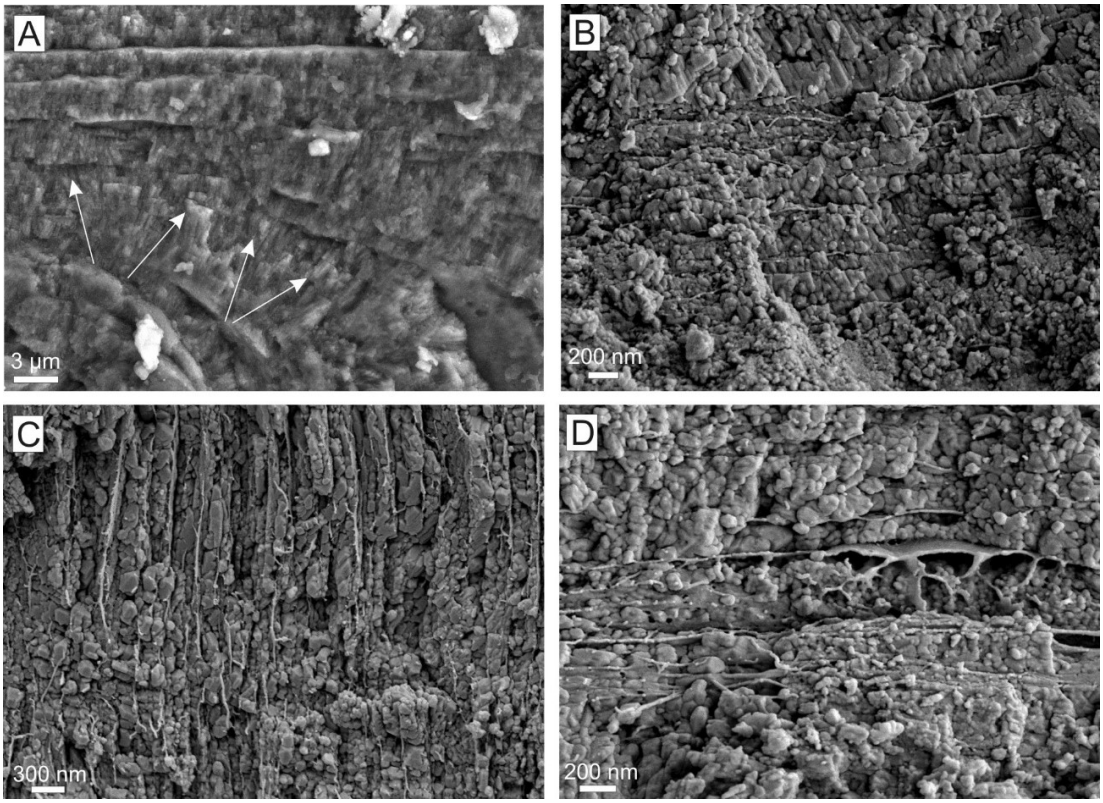

Figure 15. SEM images of fibrous and radial aragonite crystals of the prong. (**A**) Some laminae in the apical area pinch out laterally and disappear (white arrows) (SP-14). (**B**–**D**) Fibrous aragonite crystals at nanoscale are composed of clusters of small aragonite crystalline units, which are aligned. Among these crystals there are thin organic films (SP-15).

4. Discussion: Is the Cuttlebone Prong an Analogue of the Belemnite Rostrum?

The analyses of belemnites and cuttlebones show that biomineralization was strongly controlled by the organism during its stepping growth. In the case of *Sepia*, the organic matter is present everywhere in the phragmocone, dorsal shield and prong, always in alternation between organic-rich and organic-poor layers and sublayers, which may be observed at different scales (Figures 11, 12 and 15). Despite the difficulties related to preservation of organic matter and the incidence of diagenesis, this type of growth architecture is also observed in the belemnites, as indicated by petrographic features (Figures 5 and 7–9; see the results section and Benito and Reolid, [30] and Benito et al. [31] for details) and by the distribution of Mg, Na and S contents, which are higher in the intense FL layers than in the none-to-weak FL layers [30,31].

The prismatic structure of the inner layer of the dorsal shield of the cuttlebone has been interpreted as equivalent to the inner prismatic layer of the phragmocone wall in belemnites (primordial rostrum *sensu* Fuchs [71]). The structure of the middle layer of the dorsal shield and of the prong combines organic-rich and organic-poor aragonitic elements, such as has been deduced in the belemnite rostrum after SEM and FL examination [30,31]. The outer layer of the dorsal shield cannot be compared with the rostrum solidum of belemnites, but this type of radially arranged microstructure is observed in other cephalopods, such as the *Nautilus* external shell [69] and the brood case of *Argonauta* [33,92,93].

In belemnite rostra, as indicated in the results section, calcite crystals start growing from the spherulites, which are distributed along the apical line, displaying a regular spherulitic-prismatic microstructure [31]. The spherulitic–prismatic structure of belemnite rostra was firstly described by Bandel et al. [43] in other specimens of *Hibolithes* and, after Benito et al. [31], has been confirmed in *Neohibolites minimum* and *Gonioteuthis* rostra [33,36].

Crystals become progressively longer and radially distributed until, towards the external wall of the rostrum, they convert into parallel prismatic crystals (Figure 6), which, in turn, displays an internal micro-fibrous texture (Figure 7). Benito et al. [31] interpreted that the slight variation in the orientation of the c-axis of calcite crystals during progressive growth could be the cause of the undulose extinction that is observed in belemnite rostra under PL microscopy. The slight changes in c-axis direction between neighboring calcite crystals have been subsequently confirmed in *Neohibolites minimum* [33]. Similarly, in longitudinal sections of *Sepia*, an equivalent arrangement of aragonite crystals, emerging from spherulites, becoming progressively longer and radially arranged to the outer wall of the prong, and displaying undulose extinction, has been also observed (Figure 10). Moreover, in transversal sections of the prong, a micro-fibrous texture, similar to that observed in belemnite rostra, has been also recognized (compare Figures 7F and 14). In this regard, Yancey and Garvei [56] have reported radial-prismatic and spherulitic-like aragonite crystal arrangements in *Anomalosaepia* specimens.

The concentric layering of belemnite rostra also resembles that observed in the prong of *Sepia orbignyana* and *S. officinalis* (compare Figures 7, 9H, 10F,I and 13C–E). In the studied belemnite rostra, the concentric pattern comprises an alternation of radially arranged layers, displaying weak FL, and very thin layers without radial structure, displaying intense FL. The alternation of weak and intense FL concentric layering has been interpreted as an alternation of organic-poor and organic-rich layers, respectively [30], in agreement with interpretations previously made by Sælen [44] in *Neohibolites* and *Belemnellocamax*. In the case of the *Sepia* prong, consecutive and concentric layers of aragonite crystals with radial arrangement are interlayered with organic-rich and non-radially distributed laminae. Additionally, in both belemnite rostrum and *Sepia* prong, it is observed that calcite and aragonite crystals, respectively, which are in optical continuity, cross-cut the organic-rich concentric layers (compare Figures 7, 9A–C, 10I and 14).

The presence of original organic matter in belemnites and other fossil shells has been observed or suggested by several authors [1,30,31,33,40,44,47,55,82,94–100]. In this regard, Benito et al. [31] also observed that single calcite crystals of belemnite rostra are composite (Figure 9; see the results section), interpreting that the FL was activated by organic compounds, which were incorporated into the belemnite skeleton during progressive growth, preferentially in the apical area and in some

concentric layers. This interpretation is in agreement with that given by Florek et al. [40] and Dunca et al. [99], who observed an excess of carbon in Jurassic belemnites, mainly in the apical line [40], and interpreted that organic matrix was involved in the formation of belemnite skeleton.

Based on these findings, Benito et al. [31] interpreted that belemnite rostra were originally porous (20–60% of porosity) and that crystals were formed during two different growth stages: the fluorescent sectors of the crystals formed during belemnite skeletal growth, as a product of biologically controlled mineralization, and the non-fluorescent sectors precipitated subsequently as a postmorten cement, filling the intra- and inter-crystalline porosity. In this regard, Benito et al. [31] argued that if calcite overgrowths would have precipitated while belemnites were alive, the density of the rostrum would have increased, changing their buoyancy and gravity center and making them too heavy to support the swimming animal's horizontal living posture, as suggested by Spaeth [38]. Thus, Benito et al. [31] highlighted that caution should be taken when analysing geochemically the belemnite rostra for palaeoenvironmental studies, in agreement with interpretations previously made by Benito and Reolid [30] based on geochemical data obtained from the studied belemnites. This assessment has been reinforced by Hoffmann et al. [42] and Stevens et al. [33], based on data obtained in *Belemnitella mucronate* and *Megateuthis gigantea* and in *Neohibolites minimum*, respectively.

Although it has not been possible to observe current porosity or pristine organic matter in belemnite rostra, the presence of high organic matter content together with the high porosity observed in the *Sepia* prong, mostly along the "apical area" (Figures 10F,I and 13C–E), is in agreement with the interpretation that belemnite rostra were originally porous [1,2,31,37–42]. The areas displaying the highest porosity, probably related to the higher organic matter content [40] and its decay, such as the apical line and growth rings displaying intense FL, were more susceptible for diagenetic alteration [30,31]. In this regard, the apical line commonly displays a cloudy appearance and bright orange-reddish luminescence due to diagenetic alteration [30,31,33,38,40,43,44,99]. Based on that, and on the high organic matter content observed along the apical line, Stevens et al. [33] proposed that the apical line of belemnite rostra is an original feature, most probably of organic origin. However, this is not in agreement with observations made by Bandel et al. [43] (1984), Benito et al. [31] and in this work (see Figure 6, Figure 5 of Bandel et al. [43], Figures 3A–F and 5A–D of Benito et al. [31]). As shown in these figures, primary spherulites are observed along the apical line, despite its cloudy appearance and bright luminescence, suggesting that the apical line was not fully organic, but an organic-rich area [31,40,43,99], where diagenetic fluids could easily percolate, because of its relatively higher original porosity, favoring the breakdown of the organic matter and the diagenetic alteration. This is also in agreement with observations made in the apical area of the *Sepia* prong (Figure 10F,I), which is composed of spherulites and displays high porosity, and with observations made by Yancey and Garvei [56], who reported that "the prong growth axis and the prong's median fissure of *Anomalosaepia* is less mineralized than other areas of skeleton, suggesting a high proportion of non-mineralized organic material that decayed after death.

Thus, the strong growth convergences observed between the belemnite rostra and the *Sepia* prong (Table 1) suggest that growing of belemnites occurred similarly to the growth of the prong of sepiids and that the *Sepia* prong is the analog of the belemnite rostrum solidum.

Table 1. Summary of the main convergences and divergences observed between the rostrum solidum of belemnites (BR) and the *Sepia* prong (SP).

Features	This Study		Related References	
	Convergences	Divergences	Belemnite Rostrum Solidum (BR)	Sepia Prong (SP)
Primary mineralogy		**BR**: Calcite **SP**: Aragonite	Veizer [2], Sælen [44], Podhala et al., [7], Arkhipkin et al. [47], Bandel & Spaeth [58], Rosales et al., [57]	Jeletzky [50], Dauphin [51], House [52]
Spherulitic-prismatic microestructure	Radially arranged crystals start growing from spherulites from which crystals emerge and diverge	**BR**: Spherulites observed along the apical line (Figure 6). **SP**: Spherulites observed in the apical area of the prong (Figure 10I)	Bandel et al., [43], Benito et al., [31], Stevens et al., [33], Hoffmann and Stevens [36]	Benito et al., [31]
Microfibrous texture of crystals	Radially arranged crystals displays micro-fibrous texture (Figures 7, 8 and 14).		Bandel et al., [43], Sælen [44]; Richter et al., [84], Benito and Reolid [30], Benito et al., [31]	
Relationship between the concentric and radial pattern	Concentric pattern, observed at different scales, is traversed by the radially-arranged micro-fibrous crystals.	**BR**: Concentric pattern is formed by an alternation of thin layers, displaying intense FL (organic-rich) and layers displaying internal radial micro-fibrous texture and weak FL (organic-poor) (Figure 7). **SP**: Concentric pattern is formed by an alternation of thin and organic-rich laminae and organic-poor layers comprising radially arranged aragonite crystals (Figures 10I and 13).	Sælen [44], Benito et al., [31]	
Primary porosity	High primary porosity inferred (BR) or observed (SP) along the apical area.	**BR**: Primary porosity is not preserved because it was later filled by calcite cement (Figure 9). **SP**: Primary porosity is preserved (Figure 10)	Spaeth et al., [1], Spaeth [37,38], Veizer [2], Richter et al., [39], Florek et al., [40], Benito et al., [31], Hoffmann et al., [42]	
Organic matter content	High original organic matter content inferred (BR) and observed(SP) along the apical area and in thin concentric layers	**BR**: Original organic matter is not preserved; it is inferred based on petrographic features and on geochemical data obtained in the studied BR by Benito and Reolid [30] and Benito et al. [31] (Figure 7and Figure 9). **SP**: Organic matter is preserved (Figures 13 and 15)	Müller-Stoll 1936 [82], Bandel et al., 1984 [43], Sælen [44], Florek et al., [40], Dunca et al., [100], Benito and Reolid [30], Benito et al., [31], Hoffmann et al., [42], Stevens et al., [33]	
Non-classical mineralization	Non-classical crystallization processes are proposed to be involved in the formation of *Sepia* endoskeleton		Cuif et al., [90], Benito et al., [31]	

Another question to address is how to interpret, in the *Sepia* prong, the fact that single aragonite crystals are internally composed of aligned clusters of nanometer-sized crystalline units, which are iso-orientated and include abundant organic matter inclusions (Figures 12, 13F and 15C,D). These structures resemble those observed in calcite crystals of the studied belemnite rostra (Figure 7E,F) and those reported by Cuif et al. [90] in belemnites (see Figure 7.42 of Cuif et al. [90]). These authors noted that radial prims of belemnites were internally composed of clusters of nanometer-sized iso-orientated crystalline units, suggesting that fusion of their crystal lattices formed the broader units under a non-classical crystallization process. Non-classical crystallization has been proposed as the mechanism for the biomineralization of living and fossil organisms, such as some echinoderms, corals, foraminifera and mollusks, including belemnites [31,90,101–104]. Thus, the observations made in *Sepia* also suggest that non-classical crystallization is probably involved in the growth of their cuttlebone. These observations also suggest the possibility that small, biologically controlled and iso-orientated aragonite crystalline units were fused into larger crystals, leaving intra- and inter-crystalline pore spaces, similarly to what has been interpreted for belemnites [31,90].

5. Conclusions

The analyses of Jurassic belemnites (*Hibolithes*, *Belemnopsis* and *Passaloteuthis*) and cuttlebones (from *Sepia officinalis* and *S. orbignyana*) show that biomineralization of these shells was strongly related with the presence of organic matter in their structure. The organic matter in the cuttlebones is present in the phragmocone, dorsal shield and prong, always in alternation between organic-rich and organic-poor layers. In the case of belemnite rostra the organic matter is not directly observed, but the epifluorescence and BSEM pattern, the distribution of Mg, Na and S content and the pattern observed when rostrum solidum is etched with glutardialdehyde, indicates that organic matter was incorporated into the belemnite skeleton during progressive growth, preferentially in the apical area and in some concentric layers. Similarly, organic-rich and organic-poor (aragonite-rich) concentric layers of aragonite crystals are interlayered in the *Sepia* prong.

In belemnite rostra, calcite crystals start growing from spherulitic centers of growth, developed along the apical line, from which calcite crystals emerge and diverge becoming larger and prismatic towards the external wall of the rostra. These calcite crystals traverse the concentric growth layering of the rostra, display undulose extinction, and internal micro-fibrous texture. This microstructure resemble that observed in the prong of *Sepia*.

Additionally, the presence of high organic matter content together with the high porosity observed in the *Sepia* prong, mostly along the "apical area" is consistent with the interpretation that belemnite rostra were originally porous, that the areas displaying the highest porosity (the apical area and the organic-rich concentric layers) were more suitable for diagenetic alteration, and that caution should be taken when analysing geochemically belemnites for performing palaeoenvironmental interpretations.

The strong growth convergences observed between the belemnite rostra and the *Sepia* prong suggest that growing of belemnites occurred similarly to the growth of the prong of sepiids and that the *Sepia* prong is the analog of the belemnite rostrum solidum.

Finally, the fact that single aragonite crystals of the *Sepia* prong are internally composed of aligned clusters of nanometer-sized crystalline units, which are iso-orientated and contain abundant organic matter, suggest non-classical crystallization, as has been previously interpreted for other living and fossil organisms.

Supplementary Materials: The following are available online at http://www.mdpi.com/2075-163X/10/8/713/s1, Table S1: List of samples studied in this research.

Author Contributions: M.I.B. and M.R. conducted field sampling for belemnites and selection of cuttlebones from fish shops. M.I.B. and M.R. analyzed thin sections under petrographic microscope and SEM. M.I.B. studied the cathodoluminescence and epifluorescence of cuttlebones and belemnites. M.I.B. prepared etching of belemnites with glutardialdehyde. The two authors discussed the analytical results and prepared the manuscript and figures. All authors have read and agreed to the published version of the manuscript.

Funding: This research was carried out with the financial support of the projects CGL2014-52670, PGC2018-094034-B-C21), and by the "Sedimentary Geology, Palaeoclimate and Environmental Change" research group of the Complutense University of Madrid and RNM-200 (University of Jaén, Junta de Andalucía).

Acknowledgments: We are thankful to Sonia Campos for field assistance, to for its critical review, to Antonio Piedra, Beatriz Moral, Aitor Antón and Juan Carlos Salamanca for thin-sections preparation, to Alfredo Larios, Xabier Arroyo and Amparo Morales for their technical assistance with microprobe and scanning electron microscopy. We would like to thank the helpful observations of three anonymous reviewers.

Conflicts of Interest: The authors declare no conflict of interest.

References

1. Spaeth, C.H.R.; Hoefs, J.; Vetter, U. Some aspects of isotopic composition of belemnites and related paleotemperatures. *GSA Bull.* **1971**, *82*, 3139–3150. [CrossRef]
2. Veizer, J. Chemical diagenesis of belemnite shells and possible consequences for paleotemperature determinations. *N. Jahrb. Geol. Paläont. Abh.* **1974**, *147*, 91–111.
3. Price, G.D.; Sellwood, B.W. Palaeotemperatures indicated by Upper Jurassic (Kimmeridgian Tithonian) fossils from Mallorca determined by oxygen isotope composition. *Palaeogeogr. Palaeoclimatol. Palaeoecol.* **1994**, *110*, 1–10. [CrossRef]
4. Price, G.D.; Sellwood, B.W. "Warm" palaeotemperatures from high Late Jurassic palaeolatitudes (Falkland Plateau): Ecological, environmental or diagenetic controls? *Palaeogeogr. Palaeoclimatol. Palaeoecol.* **1997**, *129*, 315–327. [CrossRef]
5. Jones, C.E.; Jenkyns, H.C.; Coe, A.L.; Hesselbo, S.P. Sr-isotopic variations in Jurassic and Cretaceous seawater. *Geochim. Cosmochim. Acta* **1994**, *58*, 3061–3074. [CrossRef]
6. Jones, C.E.; Jenkyns, H.C.; Hesselbo, S.P. Strontium isotopes in Early Jurassic seawater. *Geochim. Cosmochim. Acta* **1994**, *58*, 1285–1301. [CrossRef]
7. Podhala, O.G.; Mutterlose, J.; Veizer, J. Preservation of $\delta^{18}O$ and $\delta^{13}C$ in belemnite rostra from the Jurassic/Early Cretaceous successions. *Am. J. Sci.* **1998**, *298*, 324–347. [CrossRef]
8. Veizer, J.; Ala, D.; Azmy, K.; Bruckschen, P.; Buhl, D.; Bruhn, F.; Carden, G.A.F.; Diener, A.; Ebneth, S.; Godderis, Y.; et al. $^{87}Sr/^{86}Sr$, ^{13}C and ^{18}O evolution of Phanerozoic seawater. *Chem. Geol.* **1999**, *161*, 59–88. [CrossRef]
9. McArthur, J.M.; Donovan, D.T.; Thirlwall, M.F.; Fouke, B.W.; Mattey, D. Strontium isotope profile of the early Toarcian (Jurassic) ocean anoxic event, the duration of ammonite biozones, and belemnite palaeotemperatures. *Earth Planet. Sci. Lett.* **2000**, *179*, 269–285. [CrossRef]
10. Niebuhr, B.; Joachimski, M.M. Stable isotope and trace element geochemistry of Upper Cretaceous carbonates and belemnite rostra (Middle Campanian, north Germany). *Geobios* **2002**, *35*, 51–64. [CrossRef]
11. Price, G.D.; Gröcke, D.R. Strontium-isotope stratigraphy and oxygen- and carbon-isotope variation during the Middle Jurassic-Early Cretaceous of the Falkland Plateau, South Atlantic. *Palaeogeogr. Palaeoclimatol. Palaeoecol.* **2002**, *183*, 209–222. [CrossRef]
12. Rosales, I.; Quesada, S.; Robles, S. Paleotemperature variations of Early Jurassic seawater recorded in geochemical trends of belemnites from the Basque-Cantabrian basin, northern Spain. *Palaeogeogr. Palaeoclimatol. Palaeoecol.* **2004**, *203*, 253–275. [CrossRef]
13. Rosales, I.; Robles, S.; Quesada, S. Elemental and oxygen isotope composition of Early Jurassic belemnites: Salinity vs. temperature signals. *J. Sediment. Res.* **2004**, *74*, 342–354. [CrossRef]
14. Wierzbowski, H. Carbon and oxygen isotope composition of Oxfordian-Early Kimmeridgian belemnite rostra: Palaeoenvironmental implications for Late Jurassic seas. *Palaeogeogr. Palaeoclimatol. Palaeoecol.* **2004**, *203*, 153–168. [CrossRef]
15. Wierzbowski, H.; Dembicz, K.; Praszkier, T. Oxygen and carbon isotope composition of Callovian-Lower Oxfordian (Middle-Upper Jurassic) belemnite rostra from central Poland: A record of a Late Callovian global sea-level rise? *Palaeogeogr. Palaeoclimatol. Palaeoecol.* **2009**, *283*, 182–194. [CrossRef]
16. Nieto, L.M.; Ruiz-Ortiz, P.A.; Rey, J.; Benito, M.I. Sr-Isotope Stratigraphy (SIS) elucidates the age of condensed levels: Examples from the Subbetic (Southern Spain). *Sedimentology* **2008**, *55*, 1–29.
17. Price, G.D.; Rogov, M.A. An isotopic appraisal of the Late Jurassic greenhouse phase in the Russian Platform. *Palaeogeogr. Palaeoclimatol. Palaeoecol.* **2009**, *273*, 41–49. [CrossRef]

18. Alberti, M.; Fürsich, F.T.; Pandey, D.K.; Ramkumar, M. Stable isotope analyses of belemnites from the Kachchh Basin, western India: Paleoclimatic implications for the Middle to Late Jurassic transition. *Facies* **2011**, *18*. [CrossRef]
19. Prokoph, A.; Shields, G.A.; Veizer, J. Compilation and time-series analysis of a marine carbonate $\delta^{18}O$, $\delta^{13}C$, $^{87}Sr/^{86}Sr$ and $\delta^{34}S$ database through Earth history. *Earth Sci. Rev.* **2008**, *87*, 113–133. [CrossRef]
20. Nunn, E.V.; Price, G.D.; Hart, M.B.; Page, K.N.; Leng, M.J. Isotopic signals from Callovian-Kimmerdgian (Middle-Upper Jurassic) belemnite and bulk organic carbon, Staffin Bay, Isle of Skye, Scotland. *J. Geol. Soc. Lond.* **2009**, *166*, 633–641. [CrossRef]
21. Nunn, E.V.; Price, G.D. Late Jurassic (Kimmeridgian-Tithonian) stable isotopes ($\delta^{18}O$, $\delta^{13}C$) and Mg/Ca ratios: New palaeoclimate data from Helmsdale, northeast Scotland. *Palaeogeogr. Palaeoclimatol. Palaeoecol.* **2010**, *292*, 325–335. [CrossRef]
22. Wierzbowski, H.; Rogov, M. Reconstructing the palaeoenvironment of the Middle Russian Sea during the Middle–Late Jurassic transition using stable isotope ratios of cephalopod shells and variations in faunal assemblages. *Palaeogeogr. Palaeoclimatol. Palaeoecol.* **2011**, *299*, 250–264. [CrossRef]
23. Li, Q.; McArthur, J.M.; Atkinson, T.C. Lower Jurassic belemnites as indicators of palaeo-temperature. *Palaeogeogr. Palaeoclimatol. Palaeoecol.* **2011**, *315–316*, 38–45. [CrossRef]
24. Veizer, J.; Prokoph, A. Temperatures and oxygen isotopic composition of Phanerozoic oceans. *Earth-Sci. Rev.* **2015**, *146*, 92–104. [CrossRef]
25. Ait-Itto, F.Z.; Price, G.D.; Ait Addi, A.; Chafiki, D.; Mannani, I. Bulk-carbonate and belemnite carbon-isotope records across the Pliensbachian-Toarcian boundary on the northern margin of Gondwana (Issouka, Middle Atlas, Morocco). *Palaeogeogr. Palaeoclimatol. Palaeoecol.* **2017**, *466*, 128–136. [CrossRef]
26. Wierzbowski, H.; Bajnai, D.; Wacker, U.; Rogov, M.A.; Fiebig, J.; Tesakova, E.M. Clumped isotope record of salinity variations in the Subboreal Province at the Middle-Late Jurassic transition. *Glob. Planet. Chang.* **2018**, *167*, 172–189. [CrossRef]
27. Rosales, I.; Barnolas, A.; Goy, A.; Sevillano, A.; Armendariz, M. Isotope records (C-O-Sr) of late Pliensbachian-early Toarcian environmental perturbations in the westernmost Tethys (Majorca Island, Spain). *Palaeogeogr. Palaeoclimatol. Palaeoecol.* **2018**, *497*, 168–185. [CrossRef]
28. Ebel, K. Zur Schwimmf¨ahigkeit von Belemniten. *Paläontol. Z.* **1987**, *61*, 229–251. [CrossRef]
29. Monks, N.; Hardwick, J.D.; Gale, A.S. The function of the belemnite guard. *Paläontol. Z.* **1996**, *70*, 425–431. [CrossRef]
30. Benito, M.I.; Reolid, M. Belemnite taphonomy (Upper Jurassic, Western Tethys) Part II: Fossil-diagenetic analysis including combined petrographic and geochemical techniques. *Palaeogeogr. Palaeoclimatol. Palaeoecol.* **2012**, *358–360*, 89–108. [CrossRef]
31. Benito, M.I.; Reolid, M.; Viedma, C. On the microstructure, growth pattern and original porosity of belemnite rostra: Insights from calcitic Jurassic belemnites. *J. Iber. Geol.* **2016**, *42*, 201–226.
32. Dera, G.; Toumoulin, A.; De Baets, K. Diversity and morphological evolution of Jurassic belemnites from South Germany. *Palaeogeogr. Palaeoclimatol. Palaeoecol.* **2016**, *457*, 80–97. [CrossRef]
33. Stevens, K.; Griesshaber, E.; Schmahl, W.; Casella, L.; Iba, Y.; Mutterlose, J. Belemnite biomineralization, development, and geochemistry: The complex rostrum of *Neohibolites Minimus*. *Palaeogeogr. Palaeoclimatol. Palaeoecol.* **2017**, *468*, 388–402. [CrossRef]
34. Rita, P.; De Baets, K.; Schlott, M. Rostrum size differences between Toarcian belemnite battlefields. Mitteilungen aus dem Museum für Naturkunde in Berlin. *Foss. Rec.* **2018**, *21*, 171–182. [CrossRef]
35. Rita, P.; Nätscher, P.; Duarte, L.V.; Weis, R.; De Baets, K. Mechanisms and drivers of belemnite body-size dynamics across the Pliensbachian–Toarcian crisis. *R. Soc. Open Sci.* **2019**, *6*, 190494. [CrossRef]
36. Hoffmann, R.; Stevens, K. The palaeobiology of belemnites—Foundation for the interpretation of rostrum geochemistry. *Biol. Rev.* **2020**, *95*, 94–123. [CrossRef]
37. Spaeth, C.H.R. Weitere Untersuchungen der Primär- und Fremdstrukturen in calcitischen und aragonitischen Schalenlagen englischer Unterkreide-Belemniten. *Paläontol. Z.* **1973**, *47*, 163–174. [CrossRef]
38. Spaeth, C.H.R. Zur Frage der Schwimmverhältnisse bei Belemniten in Abhängigkeit vom Primärgefüge der Hartteile. *Paläontol. Z.* **1975**, *49*, 321–331. [CrossRef]
39. Richter, D.K.; Götte, T.; Götze, J.; Neuser, R.D. Progress in application of cathodoluminescence (CL) in sedimentary petrology. *Mineral. Petrol.* **2003**, *79*, 127–166. [CrossRef]

40. Florek, M.; Youn, H.S.; Ro, C.; Wierzbowski, H.; Osán, J.; Kazimierczak, W.; Kuczumow, A. Investigation of chemical composition of belemnite rostra by synchrotron-based X-ray microfluorescence and diffraction and electron microprobe. *J. Alloys Compd.* **2004**, *362*, 99–106. [CrossRef]
41. Ullmann, C.V.; Frei, R.; Korte, C.; Hesselbo, S.P. Chemical and isotopic architecture of the belemnite rostrum. *Geochem. Cosmochim. Acta* **2015**, *159*, 231–243. [CrossRef]
42. Hoffman, R.; Richter, D.K.; Neuser, N.; Jöns, B.J.; Lemanis, R.E.; Fusseis, F.; Xiao, X.; Immenhauser, A. Evidence for a composite organic-inorganic fabric of belemnite rostra: Implications for palaeoceanography and palaeoecology. *Sediment. Geol.* **2016**, *341*, 203–251. [CrossRef]
43. Bandel, K.; Engeser, T.; Reitner, J. Die Embryonal Entwicklung von *Hibolithes* (Be1emnitida, Cephalopoda). *N. Jahrb. Geol. Paläont. Abh.* **1984**, *167*, 275–303.
44. Sælen, G. Diagenesis and construction of the belemnite rostrum. *Palaeontology* **1989**, *32*, 765–798.
45. Kröger, B.; Vinther, J.; Fuchs, D. Cephalopod origin and evolution: A congruent picture emerging from fossils, development and molecules: Extant cephalopods are younger than previously realised and were under major selection to become agile, shell-less predators. *Bioessays* **2011**, *33*, 602–613. [CrossRef] [PubMed]
46. Fuchs, D.; Iba, Y.; Ifrim, C.; Nishimura, T.; Kennedy, W.J.; Keupp, H.; Tanabe, K. *Longibelus* gen. nov., a new Cretaceous coleoid genus linking Belemnoidea and early Decabrachia. *Palaeontology* **2013**, *56*, 1081–1106.
47. Arkhipkin, A.I.; Bizikov, V.A.; Fuchs, D. Vestigial phragmoconoe in the gladius points to a deepwater origin of squid (Mollusca: Cephalopoda). *Deep Sea Res. Part I* **2012**, *61*, 109–122. [CrossRef]
48. Rexfort, A.; Mutterlose, J. Stable isotope records from *Sepia officinalis*: A key to understanding the ecology of belemnites? *Earth Planet. Sci. Lett.* **2006**, *247*, 212–221. [CrossRef]
49. Mutterlose, J.; Malkoc, M.; Schouten, S.; Sinninghe Damsté, J.P.; Forster, A. TEX_{86} and stable $d^{18}O$ paleothermometry of early Cretaceous sediments: Implications for belemnite ecology and paleotemperature proxy application. *Earth Planet. Sci. Lett.* **2010**, *298*, 286–298. [CrossRef]
50. Jeletzky, J.A. Paleontological Contributions. In *Comparative Morphology, Phylogeny, and Classification of Fossil Coleoidea. Mollusca, Article 7*; University of Kansas: Lawrence, KS, USA, 1966; pp. 1–162.
51. Dauphin, Y. Microstructures des Céphalopodes. IV Le "rostre" de Belosepia (Dibranchiata). *Paläontol. Z.* **1984**, *58*, 99–117. [CrossRef]
52. House, M.R. Major features of Cephalopod evolution. In *Cephalopods: Present and Past*; Wiedman, J., Kullmann, J., Eds.; University of Kansas Press: Lawrence, KS, USA, 1988; pp. 1–16.
53. Adam, W.; Rees, W.J. A Review of the Cephalopod Family Sepiidae. British Museum (Natural History), The John Murray Expedition 1933–34. *Sci. Rep.* **1966**, *11*, 1–165.
54. Bandel, K.; Boletzky, S.V. A comparative study of the structure, development and morphological relationships of chambered cephalopod shells. *Veliger* **1979**, *21*, 313–354.
55. Yancey, T.E.; Garvie, C.L.; Wicksten, M. The middle Eocene *Belosaepia ungula* (Cephalopoda: Coleoida) from Texas: Structure, ontogeny and function. *J. Paleont.* **2010**, *84*, 267–287. [CrossRef]
56. Yancey, T.E.; Garvie, C.L. Redescription of *Anomalosaepia* (Cephalopoda: Coleoida): A sepioid with a bimineralic calcite and aragonite skeleton. *J. Paleont.* **2011**, *85*, 904–915. [CrossRef]
57. Rosales, I.; Quesada, S.; Robles, S. Primary and diagenetic isotopic signal in fossils and hemipelagjc carbonates: The Lower Jurassic of northern Spain. *Sedimentology* **2001**, *48*, 1149–1169. [CrossRef]
58. Bandel, K.; Spaeth, C. Structural differences in the ontogeny of some belemnite rostra. In *Cephalopods: Present and Past*; Wiedmann, J., Kullmann, J., Eds.; Schweizerbart'sche Verlagschhandlung: Stuttgart, Germany, 1988; pp. 247–271.
59. Doguzhaeva, L.A. The original composition of the Pro-ostracum of an Early Sinemurian belemnite from Belgium deduced from mode of fossilization and ultrastructure. *Palaeontology* **2012**, *55*, 249–260. [CrossRef]
60. Engeser, T.; Reitner, J. *Chitinobelus acifer* Fischer 1981, ein Belemnoteuthide (Coleoidea) mit epirostrom. *N. Jahrb. Geol. Paläont. Abh.* **1983**, *161*, 496–501.
61. Naydin, D.P.; Barskov, I.S.; Kiyachko, S.I. Aragonitic and calcitic composition of the belemnitid rostra from Upper Cretaceous of the western Taymyr: Stable isotopic composition of oxygen and carbon. *Paleontol. Žurnal.* **1987**, *3*, 3–8.
62. Bandel, K.; Kulicki, C. *Belemnoteuthis polonica*: A belemnite with an aragonitic rostrum. In *Cephalopods: Present and Past*; Wiedmann, J., Kullmann, J., Eds.; Schweizerbart'sche Verlagschhandlung: Stuttgart, Germany, 1988; pp. 303–316.

63. Doyle, P.; Shakides, E. The Jurassic Belemnite Suborder Belemnotheutina. *Palaeontology* **2004**, *47*, 983–998. [CrossRef]
64. Dauphin, Y.; Williams, C.T.; Barskov, I.S. Aragonitic rostra of the Turonian belemnitid *Goniocamax*: Arguments from diagenesis. *Acta Palaeont. Pol.* **2007**, *52*, 85–97.
65. Naef, A. *Die fossilen Titenfische*; Verlag von Gustav Fischer: Jena, Germany, 1922; pp. 1–322.
66. Abel, O. *Palaobiologie der cephalopoden aus der Gruppe der Dibranchiaten*; Verlag von Gustav Fischer: Jena, Germany, 1916; pp. 1–289.
67. Krymgol'ts, G.Y. Subclass Endocochlia. In *Principles of Paleontology. Mollusca-Cephalopoda 2*; Luppov, N.P., Drushchits, V.V., Eds.; Gosgeoltekhizdat: Moscow, Russia, 1958; pp. 145–178. (In Russian)
68. Naydin, D.P. *Morphology and Paleobiology of Upper Cretaceous Belemnites*; Izd-vo Moskov University: Moscow, Russia, 1969; pp. 1–302. (In Russian)
69. Barskov, I.S. Mikrostruktura sloyev skeletal sepia I spiruly I ikh sopostavleniye so sloyami rakoviny drugokh mollyuskov. *Paleontol. Žurnal.* **1973**, *3*, 3–13.
70. Dauphin, Y. Implications of a microstructural comparison in some fossil and recent coleoid cephalopod shells. *Palaeontogr. Abteilung A* **1985**, *191*, 69–83.
71. Fuchs, D. The "rostrum"-problem in coleoid terminology: An attempt to clarify inconsistencies. *Geobios* **2012**, *45*, 29–39. [CrossRef]
72. Košťák, M.; Jagt, J.W.M.; Speijer, R.P.; Stassen, P.; Steurbaut, E. New Paleocene sepiid coleoids (Cephalopoda) from Egypt: Evolutionary significance and origin of the sepiid 'rostrum'. *PLoS ONE* **2013**, *8*, e81180.
73. Bizikov, V.A. Evolution of the Shell in Cephalopoda. In *Ruthenica*; VNIRO Publishing: Moscow, Russia, 2008.
74. Bandel, K. Cephalopod shell structure and general mechanisms of shell formation. In *Skeletal Biomineralization: Patterns, Processes and Evolutionary Trends*; Carter, J.G., Reinhold, V.N., Eds.; Wiley: New York, NY, USA, 1990; pp. 97–115.
75. Doguzhaeva, L.A. A rare coleoid mollusc from the upper Jurassic of central Russia. *Acta Palaeont. Pol.* **2000**, *45*, 389–406.
76. Bettencourt, V.; Guerra, A. Carbon-and oxygen-isotope composition of the cuttlebone of *Sepia officinalis*: A tool for predicting ecological information? *Mar. Biol.* **1999**, *133*, 651–657. [CrossRef]
77. Rexfort, A.; Mutterlose, J. The role of biogeography and ecology on the signature of cuttlefishes (Cephalopoda, Sepiidae) and the impact on belemnite studies. *Palaeogeogr. Palaeoclimatol. Palaeoecol.* **2009**, *284*, 153–163. [CrossRef]
78. Reolid, M.; Mattioli, E.; Nieto, L.M.; Rodríguez-Tovar, F.J. The Early Toarcian Ocanic Anoxic Event in the External Subbetic (Southiberian Palaeomargin, Westernmost Tethys): Geochemistry, nannofossils and ichnology. *Palaeogeogr. Palaeoclimatol. Palaeoecol.* **2014**, *411*, 79–94. [CrossRef]
79. Iversen, T.H. *Elektronmikroskopi*; Tapir Forlag: Trondheim, Norway, 1973; 108p.
80. Sabatini, D.D.; Miller, F.; Barnet, R.J. Aldehyde fixation for morphological and enzyme histochemical studies with the electron microscope. *J. Histochem. Cytochem.* **1964**, *12*, 57. [CrossRef]
81. Doguzhaeva, L.A.; Weis, R.; Delsate, D.; Mariotti, N. Embryonic shell structure of Early-Middle Jurassic belemnites, and its significance for belemnite expansion and diversification in the Jurassic. *Lethaia* **2014**, *47*, 49–65. [CrossRef]
82. Müller-Stoll, H. Beitrage zur Anatomie der Belemnoidea. *Nova Acta Leopoldina Neue Serie* **1936**, *4*, 159–226.
83. Wierzbowski, H. Life span and growth rate of Middle Jurassic mesohibolitid belemnites deduced from rostrum microincrements. *Volumina Jurassica* **2013**, *11*, 1–18.
84. Richter, D.; Nauser, R.D.; Schreuer, J.; Gies, H.; Imenhauser, A. Radiaxial-fibrous calcites: A new look at an old problem. *Sed. Geol.* **2011**, *239*, 23–36. [CrossRef]
85. Gutowska, M.A.; Melzner, F.; Pörtner, H.O.; Meier, S. Cuttlebone calcification increases during exposure to elevated seawater *p*CO2 in the cephalopod *Sepia officinalis*. *Mar. Biol.* **2010**, *157*, 1653–1663. [CrossRef]
86. Florek, M.; Fornal, E.; Gómez-Romero, P.; Zieba, E.; Paszkowicz, W.; Lekki, J.; Nowak, J.; Kuczumow, A. Complementary microstructural and chemical analyses of Sepia officinalis endoskeleton. *Mater. Sci. Eng. C* **2009**, *29*, 1220–1226. [CrossRef]
87. Checa, A.G.; Cartwrght, J.H.E.; Sánchez-Almazo, I.; Andrade, J.P.; Ruiz-Raya, F. The cuttlefish Sepia officinalis (Sepiidae, Cephalopoda) constructs cuttlebone from a liquid-crystal precursor. *Sci. Rep.* **2015**, *5*, 11513. [CrossRef]

88. Birchall, J.D.; Thomas, N.L. On the architecture and function of cuttlefish bone. *J. Mater. Sci.* **1983**, *18*, 2081–2086. [CrossRef]
89. Sherrard, K.M. Cuttlebone morphology limits habitat depth in eleven species of *Sepia* (Cephalopoda: Sepiidae). *Biol. Bull.* **2000**, *198*, 404–414. [CrossRef]
90. Cuif, J.-P.; Dauphin, Y.; Sorauf, J.E. *Biominerals and Fossils Through Time*; Cambridge University Press: Cambridge, UK, 2011; 504p.
91. Dauphin, Y. Microstructures des coquilles de Céphalopodes. II—La seighe (Dibranchiata Decapoda). *Paleontol. Abteilung* **1981**, *176*, 35–51.
92. Hewitt, R.A.; Westermann, G.E. Recurrences of hypotheses about ammonites and *Argonauta*. *J. Paleont.* **2003**, *77*, 792–795. [CrossRef]
93. Stevens, K.; Iba, Y.; Suzuki, A.; Mutterlose, J. Biological and environmental signals recorded in shells of *Argonauta argo* (Cephalopoda, Octobrachia) from the Sea of Japan. *Mar. Biol.* **2015**, *162*, 2203–2215. [CrossRef]
94. Drozdova, T.V. Organic matter of belemnites. *Geokhimia* **1969**, 1281–1285.
95. Barskov, I.S. Structure of the belemnitid rostrum. *Paleontol. J.* **1970**, *4*, 110–112.
96. Westbroek, P.; Van der Meide, P.H.; Van der Wey-Kloppers, J.S.; Van der Sluis, R.J.; De Leeuw, J.W.; de Jong, E.W. Fossil macromolecules from cephalopod shells: Characterization, immunological response and diagenesis. *Paleobiology* **1979**, *5*, 151–167. [CrossRef]
97. Clark, G.R., II. Organic matrix taphonomy in some molluscan shell microstructures. *Palaeogeogr. Palaeoclimatol. Palaeoecol.* **1999**, *149*, 305–312. [CrossRef]
98. Clark, G.R., II. Organic matrix in the porifera and cnidaria: Déjà vu through a temporal telescope. *Geol. Soc. Am. Abstr. Progr.* **2005**, *37*, 366.
99. Dunca, E.; Doguzhaeva, L.; Schöne, B.R.; Schootbrugge, B. Growth patterns in rostra of the Middle Jurassic belemnite *Megateuthis giganteus*: Controlled by the moon? *Acta Univ. Carol. Geol.* **2006**, *49*, 107–117.
100. Wierzbowski, H.; Joachimski, M.M. Stable isotopes, elemental distribution, and growth rings of belemnopsid belemnite rostra: Proxies for belemnite life habitat. *Palaios* **2009**, *24*, 377–386. [CrossRef]
101. Weiner, S.; Mahamid, J.; Politi, Y.; Ma, Y.; Addadi, L. Overview of the amorphous precursor phase strategy in biomineralization. *Front. Mater. Sci. Chin.* **2009**, *3*, 104–108. [CrossRef]
102. Cölfen, H.; Antonietti, M. *Mesocrystals and Non-Classical Mineralization*; John Wiley & Sons, Ltd.: London, UK, 2008; 276p.
103. Marin, F.; Narayanappa, P.; Motreuil, S. Acidic Shell proteins of the mediterranean fan mussel *Pinna nobilis*. In *Progress in Molecular and Subcellular Biology: Marine Molecular Biotechnology*; Müller, W.E.G., Ed.; Springer: Berlin/Heidelberg Germany, 2001; pp. 353–395.
104. Meldrum, F.C.; Cölfen, H. Controlling mineral morphologies and structures in biological and synthetic systems. *Chem. Rev.* **2008**, *108*, 4332–4432. [CrossRef] [PubMed]